

On the Evolution of the Velocity-Mass-Size Relations of Disk-Dominated Galaxies over the Past 10 Billion Years.

Aaron A. Dutton^{1,2*†}, Frank C. van den Bosch^{3,4}, Sandra M. Faber², Luc Simard⁵, Susan A. Kassin⁶, David C. Koo², Kevin Bundy^{7‡}, Jiasheng Huang⁸, Benjamin J. Weiner⁹, Michael C. Cooper^{9§}, Jeffrey A. Newman¹⁰, Mark Mozena², Anton M. Koekemoer¹¹.

¹*Department of Physics and Astronomy, University of Victoria, Victoria, BC, V8P 5C2, Canada.*

²*UCO/Lick Observatory and Department of Astronomy & Astrophysics, University of California, Santa Cruz, CA 95064, USA.*

³*Department of Physics and Astronomy, University of Utah, 115 South 1400 East, Salt Lake City, UT 84112-0830, USA.*

⁴*Astronomy Department, Yale University, P.O. Box 208101, New Haven, CT 06520-8101, USA.*

⁵*Herzberg Institute of Astrophysics, National Research Council of Canada, 5071 West Saanich Road, Victoria, BC, V9E 2E7, Canada.*

⁶*Department of Astrophysics, University of Oxford, Oxford OX1 3RH, UK.*

⁷*Astronomy Department, University of California, Berkeley, CA 94705, USA.*

⁸*Harvard-Smithsonian Center for Astrophysics, 60 Garden Street, Cambridge, MA 02138, USA.*

⁹*Steward Observatory, University of Arizona, 933 N. Cherry Avenue, Tucson, AZ 85721 USA.*

¹⁰*Department of Physics and Astronomy, University of Pittsburgh, 401-C Allen Hall, 3941 O'Hara Street, Pittsburgh, PA 15260, USA.*

¹¹*Space Telescope Science Institute, 3700 San Martin Drive, Baltimore, MD 21218, USA.*

Accepted 2010 August 17

ABSTRACT

We study the evolution of the scaling relations between maximum circular velocity, stellar mass and optical half-light radius of star-forming disk-dominated galaxies in the context of Λ CDM-based galaxy formation models. Using data from the literature combined with new data from the DEEP2 and AEGIS surveys we show that there is a consistent picture for the evolution of these scaling relations from $z \sim 2$ to $z = 0$, both observationally and theoretically. The evolution of the observed stellar scaling relations is weaker than that of the virial scaling relations of dark matter haloes, which can be reproduced, both qualitatively and quantitatively, with a simple, cosmologically-motivated model for disk evolution inside growing Navarro-Frenk-White dark matter haloes. In this model optical half-light radii are smaller, both at fixed stellar mass and maximum circular velocity, at higher redshifts. This model also predicts that the scaling relations between baryonic quantities (baryonic mass, baryonic half-mass radii, and maximum circular velocity) evolve even more weakly than the corresponding stellar relations. We emphasize, though, that this weak evolution does not imply that individual galaxies evolve weakly. On the contrary, individual galaxies grow strongly in mass, size and velocity, but in such a way that they move largely along the scaling relations. Finally, recent observations have claimed surprisingly large sizes for a number of star-forming disk galaxies at $z \simeq 2$, which has caused some authors to suggest that high redshift disk galaxies have abnormally high spin parameters. However, we argue that the disk scale lengths in question have been systematically overestimated by a factor ~ 2 , and that there is an offset of a factor ~ 1.4 between $H\alpha$ sizes and optical sizes. Taking these effects into account, there is no indication that star forming galaxies at high redshifts ($z \simeq 2$) have abnormally high spin parameters.

Key words: galaxies: evolution – galaxies: formation – galaxies: fundamental parameters – galaxies: haloes – galaxies: high redshift – galaxies: spiral

1 INTRODUCTION

In the current paradigm of galaxy formation, galaxy disks are considered to form from the accretion of gas inside hierarchically growing cold dark matter (CDM) haloes (White &

* dutton@uvic.ca

† CITA National Fellow

‡ Hubble Fellow

§ Spitzer Fellow

Rees 1978). The dark matter (DM) and gas acquire angular momentum via tidal torques in the early universe (Peebles 1969). When the gas accretes onto the central galaxy, this angular momentum may eventually halt the collapse and lead to the formation of a rotationally supported disk (Fall & Efstathiou 1980). Under the assumption that the total specific angular momentum of the precollapse gas is similar to that of the DM and is conserved during collapse, this picture leads to predictions of present-day disk sizes that are in reasonable agreement with observations (Blumenthal et al. 1984; Dalcanton et al. 1997; Mo, Mao, & White 1998; Firmani & Avila-Reese 2000; de Jong & Lacey 2000; Pizagno et al. 2005; Dutton et al. 2007).

The observational relation between the sizes of galaxy disks and their characteristic rotation velocities (the *RV* relation) provides a measure of the specific angular momentum of galaxy disks (e.g., Navarro & Steinmetz 2000). In the simplest model for disk galaxy evolution, the sizes and rotation velocities of galaxy disks are proportional to the sizes and circular velocities of their host dark matter haloes, and the evolution of disk sizes at fixed circular velocity scales inversely with the Hubble parameter (e.g., Mo, Mao, & White 1998). For a Λ CDM cosmology (with $\Omega_M = 0.3, \Omega_\Lambda = 0.7$) this simple model predicts that disks should be a factor of $\simeq 1.8$ smaller, at fixed circular velocity, at $z = 1$, compared to $z = 0$, and a factor of $\simeq 3.0$ smaller at $z = 2$. For a standard CDM cosmology (with $\Omega_M = 1, \Omega_\Lambda = 0$) the predicted evolution is even stronger: a factor of $\simeq 2.8$ to $z = 1$ and a factor of $\simeq 5.2$ to $z = 2$.

Early observations indicated evolution in the *RV* relation with a scaling of $\sim (1+z)^{-1}$ out to $z \sim 1$, in agreement with theoretical expectations (Mao, Mo & White 1998). More recently, Bouché et al. (2007) found that the disk scale size-rotation velocity relation at $z \simeq 2.2$ has roughly the same zero point as at $z = 0$, in disagreement with simple theoretical expectations. While there are concerns about sample selection, small statistics, errors at high- z , etc., it is nonetheless appropriate to start thinking about the implications of this result for galaxy formation. A proposed explanation for this non-evolution is that disk galaxies at $z \simeq 2.2$ have spin parameters¹ a factor of 3 higher than those predicted by Λ CDM (Bouché et al. 2007; Burkert et al. 2009). If confirmed, this could imply a significant modification of the current paradigm of galaxy disk formation, either through a decoupling of the angular momentum of baryons and dark matter, or more drastically by changing the mechanism by which galactic angular momentum is generated.

A decoupling between the angular momentum of baryons and dark matter haloes is actually seen in cosmological hydrodynamical simulations of disk galaxy formation (e.g., Navarro & Steinmetz 2000; Sales et al. 2009; Piontek & Steinmetz 2009). However, the result is that baryons lose angular momentum to the halo, which only makes high disk spin parameters harder to explain. A possible mechanism for increasing the specific angular momentum of disk galaxies is the removal of material with low specific angular momentum through galactic outflows. This mechanism has been shown theoretically to be effective in

¹ The spin parameter is a dimensionless measure of the specific angular momentum of dark matter halos.

dwarf galaxies (Maller & Dekel 2002; Dutton 2009; Governato et al. 2010). Galactic outflows appear ubiquitous in star forming galaxies at redshift $z \sim 3$ (Shapley et al. 2003) and $z = 1.4$ (Weiner et al. 2009). But whether they are powerful enough to increase the specific angular momentum of massive ($V_{\text{rot}} = 200 \text{ km s}^{-1}$) galaxy disks by a whole factor of 3 remains to be seen.

The relation between galaxy size and stellar mass (the *RM* relation) of disk-dominated galaxies also shows only weak evolution to $z = 1$ (Barden et al. 2005). This weak evolution can be understood in the Λ CDM scenario as a consequence of the increase of dark halo concentrations since $z = 1$ (Somerville et al. 2008) and also because individual disk galaxies tend to evolve roughly *along* the *RM* relation (Firmani & Avila-Reese 2009). At higher redshifts, there is evidence of a factor of $\simeq 2$ decrease in half-light sizes of disk-dominated galaxies at fixed stellar mass between $z = 0$ and $z \simeq 2.5$ (Trujillo et al. 2006). Again, this evolution is weaker than the evolution in the halo *RM* relation, but it is in agreement with the models of Somerville et al. (2008) and Firmani & Avila-Reese (2009). We note that elliptical galaxies have been found to evolve even more strongly with redshift (e.g., Trujillo et al. 2006; van Dokkum et al. 2008), and thus there is clear evidence that galaxies of all types were smaller, at fixed stellar mass, at higher redshifts.

It is possible that the non-evolution of the *RV* relation and evolution of the *RM* relation of disk-galaxies are consistent. This would require evolution in the *MV* relation (i.e., the stellar mass Tully-Fisher relation, Tully & Fisher 1977), with higher M , at fixed V , at higher z . However, the opposite has been claimed, with $\simeq 0.4$ dex lower M_{star} at fixed V_{max} at $z \simeq 2.2$ compared to $z = 0$ (Cresci et al. 2009). Thus, the various data sets for the evolution of the *VMR* relations are inconsistent.

In this paper, we examine the *VMR* relations of disk galaxies using data from the literature as well as new results from the Deep Extragalactic Evolutionary Probe 2 survey (DEEP2, Davis et al. 2003; Newman et al. in prep). We discuss, and resolve, sources of discrepancies among the various data sets, and compare the data to predictions of a simple Λ CDM-based disk-galaxy evolution model. We show that the observations can be reproduced by a model with constant spin parameter in agreement with predictions from Λ CDM, and a constant galaxy mass fraction. Hence there is no need to invoke abnormally high spin parameters in order to explain the scaling relations of disk galaxies at $z \sim 2$. Throughout we assume a flat Λ CDM cosmology with $(\Omega_M, \Omega_\Lambda, h) = (0.3, 0.7, 0.7)$.

2 OBSERVATIONS

2.1 Evolution of the stellar mass Tully-Fisher relation

The relation between stellar mass² (or luminosity) and rotation velocity (or linewidth) is also commonly known as the Tully-Fisher relation (TF; Tully & Fisher 1977). We define the velocity as the maximum rotation velocity, V_{max} . Using

² Note that stellar mass throughout is total stellar mass, not disk stellar mass.

Table 1. Evolution of the stellar mass-velocity relation of star forming galaxies relative to $z = 0.0$, using DEEP2 data from Kassin et al. (2007).

redshift range	median z	$\Delta \log_{10} M_{\text{star}} S_{0.5}$	N
0.2-0.5	0.35	-0.06 ± 0.09	19
0.5-0.8	0.73	-0.03 ± 0.11	25
0.8-1.1	0.95	-0.15 ± 0.09	29

slit spectroscopy from the DEEP1 survey (Vogt et al. 2005; Weiner et al. 2005), together with optical and K -band imaging, Conselice et al. (2005) found that, at fixed V_{max} , stellar masses are lower by 0.07 ± 0.12 dex at $z \sim 0.45$, and lower by 0.11 ± 0.13 dex at $z \sim 0.85$, compared to the $z = 0$ relation from Bell & de Jong (2001). This weak evolution from $z \sim 1$ to $z \sim 0$ was confirmed by Kassin et al. (2007), who studied the stellar mass TF relation for a larger sample of galaxies from the DEEP2 survey, but adopting a different velocity indicator, $S_{0.5} = (0.5V_{\text{rot}}^2 + \sigma^2)^{1/2}$, which combines ordered motions (i.e., rotation, V_{rot}) and disordered motions (i.e., dispersion, σ) (Weiner et al. 2006a). This new parameter allowed inclusion of mergers and incompletely settled galaxies, which is useful at high redshifts where galaxies may be dynamically “young”.

Here we use data from Kassin et al. (2007) and calculate the evolution of stellar mass at fixed $S_{0.5}$ for galaxies with $S_{0.5} > 90 \text{ km s}^{-1}$ (i.e., $\log_{10} V_{\text{max}}/[\text{km s}^{-1}] > 2.1$) and inclinations between 45 and 70 degrees. As a comparison relation at redshift $z = 0$ we use the TF relation from Bell & de Jong (2001), corrected to a Chabrier (2003) IMF as given below in §2.3, and with V_{rot} converted into $S_{0.5}$ assuming $\sigma = 0$. We note that since the galaxies at $z = 0$ are rotation dominated, adopting a more realistic value of $\sigma \sim 10 \text{ km s}^{-1}$ (for the cold atomic hydrogen disk) for these galaxies will not change the $z = 0$ relation by any significant amount. The median offsets in stellar mass of the DEEP2 data with respect to the $z = 0$ relation, in three redshift bins from $z = 0.2$ to $z = 1.1$, are given in Table 1. These results are consistent with no evolution or at most a weak decrease in stellar masses at fixed circular velocity at higher redshifts.

A relatively strong evolution in the stellar mass TF relation since $z \sim 0.6$ has been reported by Puech et al. (2010). These authors find an increase of 0.34 dex in stellar mass at fixed velocity since $z \sim 0.6$. However, the same authors find no evidence for evolution in baryonic mass at fixed velocity (the baryonic Tully-Fisher relation) over the same redshift range. The large difference between the evolution of the stellar and baryonic TF relations implies that gas fractions evolve significantly. However, the inferred gas fractions of their galaxies at $z \sim 0.6$ are on average 30%, which is not much higher than that of local galaxies of the same mass. This implies that the evolution of the stellar mass TF relation should be only of order 0.1 dex different than that of the baryonic TF relation. The difference in evolution of 0.4 dex found by Puech et al. (2010) can thus be traced to the use of inconsistent local baryonic and stellar mass TF relations.

At even higher redshifts evidence has been reported of

significant evolution compared to redshift $z = 0$. Using data from SINS (Spectroscopic Imaging survey in the NIR with SINFONI, Förster Schreiber et al. 2009), Cresci et al. (2009) found that at fixed V_{max} , stellar masses at redshift $z \simeq 2.2$ are lower by 0.41 ± 0.11 dex compared to $z = 0$. Taken together, the observations indicate that there is a modest evolution in the zero point of the TF relation out to $z \sim 1$ and a stronger evolution from $z \sim 1$ to $z \sim 2$.

2.2 Evolution in the size-stellar mass relation

Barden et al. (2005) found that there was little or no evolution in the circularized³ optical half-light size-stellar mass relation of disk dominated galaxies (defined as having Sérsic index $n < 2.5$) from redshift $z \simeq 1$ to $z \simeq 0.1$. Trujillo et al. (2006) measured the evolution of the circularized rest-frame V -band half-light radius-stellar mass relation since $z \simeq 2.5$, finding that disk-galaxies (Sérsic index $n < 2.5$) are a factor of $\simeq 2$ smaller, at fixed M_{star} , at $z \simeq 2.5$ than at $z = 0.1$. Williams et al. (2010) measure the evolution of the circularized rest-frame I -band half-light radii of galaxies with stellar masses greater than $6.3 \times 10^{10} M_{\odot}$ from $z = 0.5$ to $z = 2$, finding strong evolution for both star-forming and non star-forming galaxies. In order to compare to $z = 0.1$ we use a mean I -band half-light size of 5.0 kpc. This has been determined using our SDSS measurements (see §2.2.3), and applying a correction of -0.06 dex to go to rest-frame I -band (see §3.4).

Here we present new results for the evolution of the disk size-stellar mass relation for blue-cloud disk dominated galaxies from redshifts $z = 1.2$ to $z = 0.1$ using high redshift data from DEEP2 (Davis et al. 2003; Newman et al. , in prep) and the All-wavelength Extended Groth Strip International Survey (AEGIS, Davis et al. 2007), and a low redshift comparison sample from the Sloan Digital Sky Survey (SDSS, York et al. 2000). The main difference of our study with respect to previous studies (e.g. Barden et al. 2005; Trujillo et al. 2006) is our use of disk sizes, rather than total sizes. We use disk sizes because our main interest in this paper is the evolution of galaxy disks. Total sizes, even for disk-dominated galaxies, depend on the bulge fraction and bulge size, and thus give a measurement that is more difficult to interpret.

2.2.1 DEEP2 data

Disk sizes have been measured using 2D bulge+disk fits using GIM2D (Simard et al. 2002). The bulge component was assumed to have a deVaucoulers profile (Sérsic $n = 4$), while the disk was assumed to be exponential (i.e., Sérsic $n = 1$). The fits were performed simultaneously on F606W (V) and F814W (I) single-orbit Hubble Space Telescope (HST) Advanced Camera for Surveys (ACS) images. The bulge and disk sizes are constrained to be the same in each filter, but the bulge and disk fluxes are free to vary. This choice has been made to maximize signal to noise, at the expense of

³ For sizes measured in elliptical apertures, the quoted size, is conventionally the major axis size, R . The circularized size is then often defined as $\sqrt{b/a}R$, where b/a is the minor to major axis ratio.

using bluer rest-frame wavelengths at higher redshifts: The central rest-frame wavelength of the images (i.e., the average of the F606W and F814W images) varies from $\simeq 500$ nm at $z = 0.4$ to $\simeq 320$ nm at $z = 1.2$. This may cause a small ($\simeq 10\%$) systematic overestimation of the sizes at higher redshifts, because disks tend to have color gradients (see §3.3). The sizes we present in this paper are major-axis (i.e., elliptical aperture) disk half-light sizes, i.e., 1.678 times the disk exponential scale length.

We use both spectroscopic and photometric redshifts between $0.2 < z < 1.4$. We use high quality (“z-quality” ≥ 3) spectroscopic redshifts from DEEP2 (Davis et al. 2003; Newman et al. , in prep), and photometric redshifts based on optical to Spitzer/IRAC photometry (J. Huang et al. , in preparation). For the spectro- z sample, stellar masses were obtained from optical to NIR spectral energy distribution (SED) fits from Bundy et al. (2006) which assumed a Chabrier (2003) initial mass function (IMF). For the photo- z sample we use stellar masses calculated using a relation between B -band stellar mass-to-light ratio and rest-frame ($U - B$) color, which we calibrate against the Bundy et al. (2006) masses. Our calibration is similar to the ones reported in Lin et al. (2007) and Weiner et al. (2009), but make use of only rest-frame ($U - B$) colors, rather than ($U - B$) and ($B - V$). We compute rest-frame ($U - B$) colors and B -band luminosities by applying kcorrect v4.1.4 (Blanton & Roweis 2007) to DEEP2 B, R, I magnitudes.

We select blue-cloud galaxies for this study by using the “green valley” in the ($U - B$) color-stellar mass plane as the division:

$$(U - B) < 1.05 - 0.1(\log_{10} M_{\text{star}} - 10). \quad (1)$$

In addition we select only disk-dominated galaxies with disk light fractions greater than 50%. This additional cut only removes a small fraction of galaxies because the vast majority of blue galaxies already have disk fractions greater than 50%. In order to minimize the effects of extinction on disk sizes, colors and stellar masses, while at the same time keeping a significant sample size, we limit our sample to galaxies with disk minor-to-major axis ratios greater than 0.5 (corresponding to disk inclinations less than 60 degrees, for a zero thickness disk).

2.2.2 Magnitude and surface brightness selection effects

The DEEP2 spectroscopic survey is limited by apparent R -band magnitude of 24.1 AB. This results in a bias against redder galaxies at low stellar masses (Willmer et al. 2006). However, the stellar masses we use from Bundy et al. (2006) are limited by apparent K -band magnitude of about 22.5 AB. This additional K -band selection is close to a selection on stellar mass and thus removes much of the bias by removing lower-mass blue galaxies from the sample. In order to remove any remaining color biases we apply an additional redshift dependent lower stellar mass limit of $\log_{10} M_{\text{min}} = 8.5 + z$. Our final DEEP2 sample consists of ~ 800 galaxies with spectro- z 's and ~ 2000 galaxies with photo- z 's.

A potentially important selection bias for galaxy size evolution studies is incompleteness at low surface brightness levels, especially at higher redshifts due to the cosmological

surface brightness dimming, which goes as $(1+z)^4$. To determine the impact of surface brightness selection effects it is customary to create model galaxies, insert them into real data, and then run the same source detection algorithms that were applied to the real data. For the single orbit *HST*/ACS F850LP observations from GEMS used by Barden et al. (2005) and Trujillo et al. (2006), these tests predict that surface brightness limits are significant for galaxies brighter than the magnitude limit of the COMBO-17 photometric redshift survey. However, as shown by Melbourne et al. (2007), typical large spiral galaxies at $z \sim 1$ have significant amounts of high-surface-brightness substructure. This makes them much easier to detect and measure spectroscopic redshifts for than smooth disks. In this paper we use galaxies detected in an effective exposure of two-orbits of *HST*/ACS imaging (single-orbit each of F606W and F814W). Based on the results of Melbourne et al. (2007) we conclude that, at the depth of our images, we are not missing significant numbers of large star forming galaxies with stellar masses greater than $\sim 10^{10} M_{\odot}$ at $z \sim 1$.

At the other extreme, small galaxies can be confused with stars, especially with ground based seeing limited imaging. However, stars can be reliably separated from galaxies based on the fact that stars tend to be brighter than compact high-redshift galaxies, and also occupy a different locus from galaxies in ($B - R, R - I$) space (Newman et al. in prep). Furthermore, there is nothing to prevent small galaxies from being in our photo- z sample. The good agreement between the size-mass relations from our spectro- z and photo- z samples vindicates the DEEP2 star-galaxy separation method. We thus conclude that our sample of star-forming galaxies from DEEP2 is unlikely to be affected by biases against very small or very large galaxies above the (redshift dependent) stellar mass limits of our sample.

2.2.3 SDSS comparison sample

As a low redshift comparison sample, we use data from the SDSS DR7 (Abazajian et al. 2009). We use a similar methodology to the DEEP2 sample in order to minimize systematic biases in the comparison between high and low redshift data. Thus, we measure *disk half-light radii* with 2D bulge+disk fits using GIM2D, performed simultaneously on g and r images with the bulge and disk sizes constrained to be the same in each filter (Simard et al. , in prep). We use galaxies with spectroscopic redshifts from $0.02 < z < 0.20$ and stellar masses calculated using the relation between r -band mass-to-light ratio and ($g - r$) color from Bell et al. (2003) with an offset of -0.1 dex to correspond to a Chabrier (2003) IMF. We select blue-cloud galaxies for this study using the valley in the ($g - r$)-stellar mass plane and requiring:

$$(g - r) < 0.71 - 0.067(\log_{10} M_{\text{star}} - 10). \quad (2)$$

As with the DEEP2 sample we select galaxies with disk light fractions greater than 50% and with disk minor-to-major axis ratios greater than 0.5 (corresponding to disk inclinations less than 60 degrees for a zero thickness disk). We use GIM2D model g and r magnitudes, with k-corrections to $z = 0$ based on SDSS petrosian *ugriz* magnitudes.

The SDSS spectroscopic survey is limited by apparent r -band magnitude. In the color-stellar mass plane this results in a bias against redder galaxies at low stellar masses. In

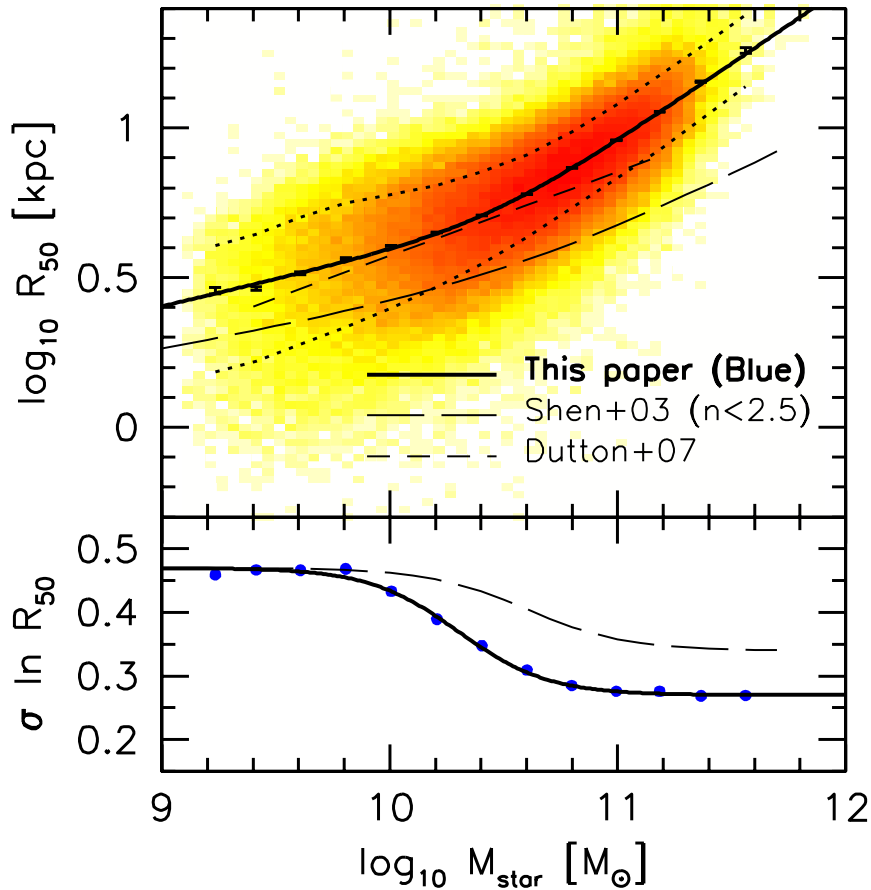


Figure 1. Disk half-light radius-stellar mass (RM) relation of blue-cloud disk-dominated galaxies (bulge fraction less than 0.5) from the SDSS. The color corresponds to the observed number density of galaxies on a logarithmic scale. The error bars show the median and error on the median in stellar mass bins of width 0.2 dex. The dotted lines show the 84th and 16th percentiles of the size distribution. The solid line shows our fit to the median relation using Eq. 3. For comparison we also show the total half-light radius-stellar mass relation of disk-dominated (Sérsic $n < 2.5$) galaxies from Shen et al. (2003, long-dashed line) and the disk half-light radius-stellar mass relation from Dutton et al. (2007, short-dashed line). The scatter in the size-mass relation is given in the lower panel. The points show our measurements from SDSS, the solid line shows our fit to these data using Eq. 4, while the long-dashed line shows the result from Shen et al. (2003).

order to remove this effect, we apply a minimum stellar mass of: $\log_{10} M_{\text{min}} = 10.4 + \log_{10}(z/0.1)$. Our final SDSS sample consists of ~ 130000 galaxies.

Fig. 1 shows the disk half-light radius-total stellar mass relation from our SDSS sample. We fit the median SDSS disk size-mass relation with the following double power-law:

$$R = R_0 \left(\frac{M}{M_0} \right)^\alpha \left[\frac{1}{2} + \frac{1}{2} \left(\frac{M}{M_0} \right)^\gamma \right]^{(\beta-\alpha)/\gamma}. \quad (3)$$

Here α is the slope at low masses ($M \ll M_0$), β is the slope at high masses ($M \gg M_0$), and γ controls the sharpness of the transition between the two slopes, M_0 is the transition mass, and R_0 is the value of R at M_0 . We find $\log_{10}(M_0/[M_{\odot}]) = 10.44$, $\log_{10}(R_0/[\text{kpc}]) = 0.72$, $\alpha = 0.18$, $\beta = 0.52$ and $\gamma = 1.8$ provide a good fit to the data.

We assume the scatter in the SDSS disk size-mass relation is log-normal with $s = \sigma_{\ln R|M}$, with the following relation:

$$s = s_2 + (s_1 - s_2) / [1 + (M/M_0)^\gamma]. \quad (4)$$

Here s_1 is the scatter at low masses, s_2 is the scatter at high masses, M_0 is the transition mass, and γ controls the sharpness of the transition. We find $s_1 = 0.47$, $s_2 = 0.27$, $\log_{10}(M_0/[M_{\odot}]) = 10.3$, and $\gamma = 2.2$ provide a good fit to the data.

For comparison, the total half-light radius-stellar mass relation for disk galaxies (Sérsic $n < 2.5$) from the SDSS study of Shen et al. (2003) is given by the long-dashed line, and the disk half-light size ($1.678 \times$ disk scale length)-stellar mass relation from Dutton et al. (2007), using the spiral galaxy sample of Courteau et al. (2007), is given by the short-dashed line. The relation from Dutton et al. (2007) is in reasonable agreement with our result considering a single power-law was used by Dutton et al. (2007). The relation from Shen et al. (2003) has a shallower slope at high masses, and is offset to smaller sizes at all masses. These differences can be understood as a consequence of two factors: circularization and bulges. The half-light radii used by Shen et al. (2003) are measured using circular apertures. Since the median major to minor axis ratio of galaxy disks

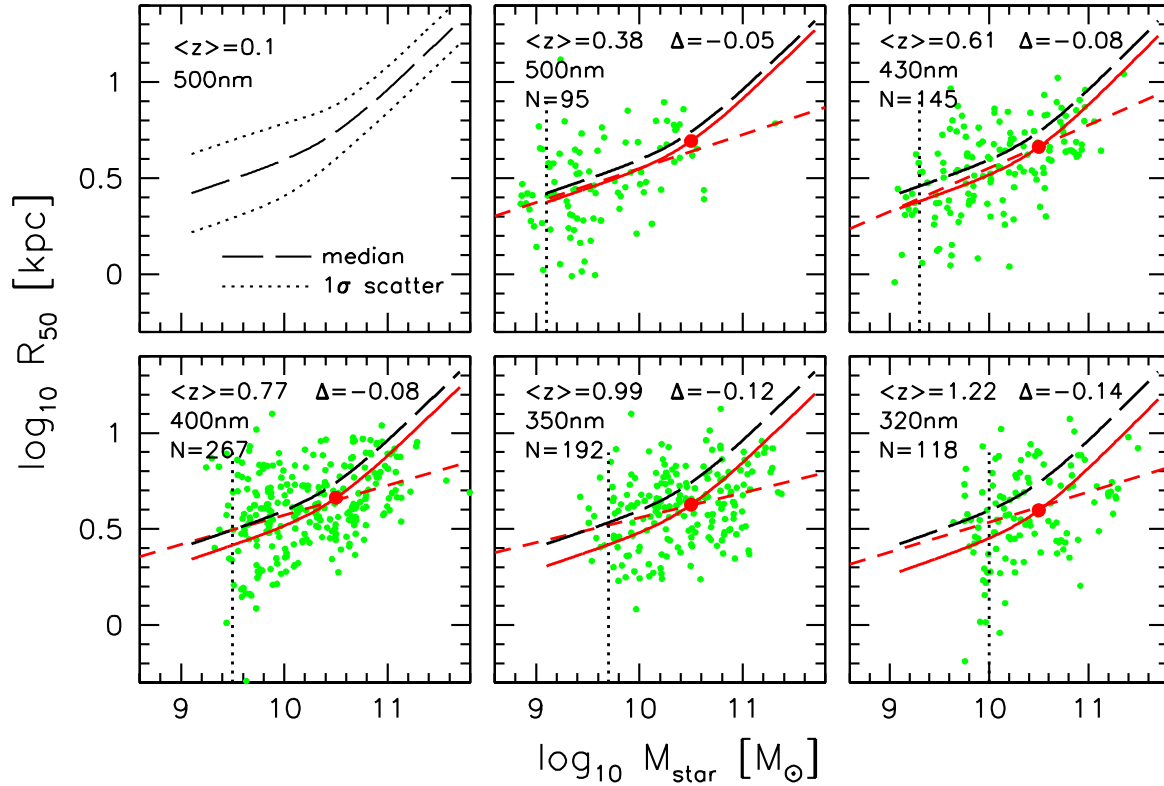


Figure 2. Evolution of the disk half-light radius-stellar mass (RM) relation of disk-dominated blue-cloud galaxies from DEEP2 using spectroscopic redshifts. The upper left panel shows the RM relation we derive for disk-dominated blue-cloud galaxies from SDSS. The long-dashed line shows the median relation, the dotted lines show 1σ scatter. In the other panels the green points show observations from DEEP2 using *HST* imaging in five redshift bins. The median redshift in each bin is given in the upper left corner of each panel, together with the central rest-frame wavelength of the imaging used to measure galaxy sizes, and the number of galaxies. The solid red line shows a fit to the DEEP2 data by offsetting the $z = 0.1$ relation (shown by the dashed line) in size. The red circle shows the median size for a stellar mass of $3 \times 10^{10} M_{\odot}$. The offset is given in the upper right corner in each panel, and is summarized in Table 2. The red short-dashed lines show a power-law fit to the data in each panel. The vertical dotted lines show the lower stellar mass limit at the upper redshift of each redshift bin.

is $\simeq 2$, a circular size measurement will underestimate the true (face-on) half-light radius by a factor of $\simeq 1.4$ (0.15 dex). This effect explains most of the discrepancy at low stellar masses. At high stellar masses there is an additional difference, which can plausibly be explained by the increased bulge fractions in higher mass galaxies (e.g. Dutton 2009). Since bulges tend to be smaller than disks, total half-light radii will be smaller than disk half-light radii.

We find that the scatter in disk sizes is mass dependent, with larger scatter at lower masses, in qualitative agreement with Shen et al. (2003). At low masses we find that the scatter of 0.47 in $\ln R$ is in agreement with Shen et al. (2003), but at high masses we find a scatter of 0.27 in $\ln R$, which is smaller than the scatter of 0.34 in $\ln R$ reported by Shen et al. (2003). As with the difference in the slopes at high masses, this difference is plausibly due to use of total half-light radii by Shen et al. (2003). We note that in the simplest Λ CDM based disk formation models (e.g., Mo, Mao, & White 1998) the scatter in disk sizes at fixed mass is equal to the scatter in the halo spin parameter, λ , which is $\sigma_{\ln \lambda} \simeq 0.5$ (e.g., Bullock et al. 2001b, Macciò et al. 2007). This is in rough agreement with the observed scatter at low stellar masses ($M_{\text{star}} \lesssim 10^{10} M_{\odot}$), but at high stellar masses

($M_{\text{star}} \gtrsim 10^{11} M_{\odot}$) the observed scatter is a factor of $\simeq 2$ lower than predicted by the simple model. This smaller than expected scatter has been noted by previous authors (e.g., de Jong & Lacey 2000; Shen et al. 2003; Pizagno et al. 2005; Dutton et al. 2007). This discrepancy may indicate that massive disk-dominated galaxies form in a subset of haloes with a biased distribution of halo spin parameters, or that the distribution of disk sizes has been modified by secular evolution (e.g., Shen et al. 2003).

2.2.4 Evolution

The evolution of the disk half-light radius-stellar mass relation in six redshift bins from $z = 0.1$ (SDSS) up to redshift $z \simeq 1.2$ (DEEP2) is shown in Figs. 2 & 3. The upper left panel shows fits to the SDSS disk size-stellar mass relation from Fig. 1. For both SDSS and DEEP2 the stellar mass is the total (i.e., disk plus bulge) stellar mass. The long-dashed line shows the median relation, and the dotted lines show the 1σ scatter.

Galaxies at redshifts $z > 0.2$ from DEEP2 are shown as green circles. The solid red lines show fits to the DEEP2 data obtained by calculating the median offset in size with

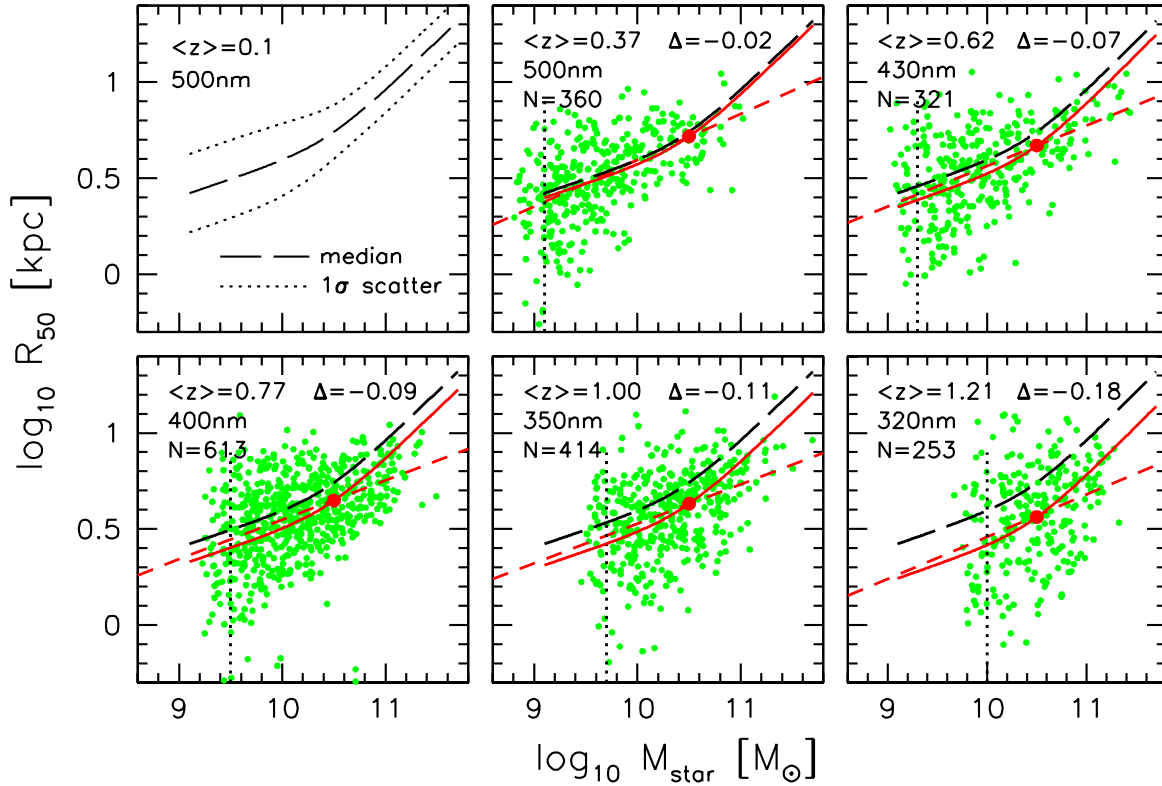


Figure 3. Evolution of the disk half-light radius-stellar mass (RM) relation of disk-dominated blue-cloud galaxies from DEEP2 using photometric redshifts. The upper left panel shows the RM relation we derive for disk-dominated blue-cloud galaxies from SDSS. The long-dashed line shows the median relation, the dotted lines show 1σ scatter. In the other panels the green points show observations from DEEP2 using HST imaging in five redshift bins. The median redshift in each bin is given in the upper left corner of each panel, together with the central rest-frame wavelength of the imaging used to measure galaxy sizes, and the number of galaxies. The solid red line shows a fit to the DEEP2 data by offsetting the $z = 0.1$ relation (shown by the dashed line) in size. The red circle shows the median size for a stellar mass of $3 \times 10^{10} M_{\odot}$. The offset is given in the upper right corner in each panel, and is summarized in Table 2. The red dashed lines show a power-law fit to the data in each panel. The vertical dotted lines show the lower stellar mass limit at the upper redshift of each redshift bin.

Table 2. Evolution of the disk half-light radius-stellar mass relation of blue-cloud disk-dominated galaxies relative to SDSS galaxies at $z = 0.1$, using data from DEEP2 from Figs. 2 & 3.

redshift range	median z	$\Delta \log_{10} R_{50} M_{\text{star}}$	N
Spectroscopic Redshifts			
0.2-0.5	0.38	-0.05 ± 0.03	95
0.5-0.7	0.61	-0.08 ± 0.02	145
0.7-0.9	0.77	-0.08 ± 0.03	267
0.9-1.1	0.99	-0.12 ± 0.02	192
1.1-1.4	1.22	-0.14 ± 0.03	118
Photometric Redshifts			
0.2-0.5	0.37	-0.02 ± 0.01	360
0.5-0.7	0.62	-0.07 ± 0.01	321
0.7-0.9	0.77	-0.09 ± 0.01	613
0.9-1.1	1.00	-0.11 ± 0.01	414
1.1-1.4	1.21	-0.18 ± 0.02	253

respect to the $z = 0.1$ relation. The offsets are given in the top right corner of each panel, and in Table 2. For

reference, the $z = 0.1$ relation is shown in each panel with black dashed lines. The short-dashed red lines show power-law fits to the data in each redshift bin. These agree well at $M_{\text{star}} \simeq 3 \times 10^{10} M_{\odot}$ (red dots in Figs. 2 & 3) but suggest the size evolution may be weaker at lower masses and stronger at higher masses.

The evolution of the zero point (size evolution at fixed M_{star}) is summarized in Fig. 4. The data from DEEP2 are shown with blue pentagons (open for photo- z , filled for spectro- z), and the data from Trujillo et al. (2006) are shown with magenta squares. Note that the latter are for total half-light radii, not disk half-light radii, but nevertheless the two data sets are consistent within the error bars. The DEEP2 data, however, shows stronger evidence for evolution both internally and in comparison to SDSS. For DEEP2 the evolution of the spectro- z sample is well fit by

$$\Delta \log_{10} R_{50} = 0.018 \pm 0.002 - 0.44 \pm 0.04 \log_{10}(1+z), \quad (5)$$

where $\Delta \log_{10} R_{50}$ is the size evolution relative to $z = 0.1$.

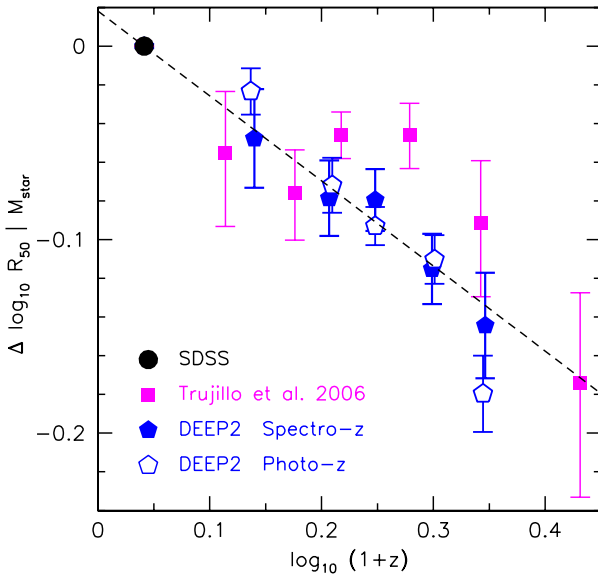


Figure 4. Evolution of the disk half-light radius-stellar mass relation of blue/disk galaxies from redshifts $z = 0.1$ to $z \simeq 1.2$. The pentagons show results for blue-cloud disk-dominated galaxies from DEEP2, where the sizes are the disk half-light sizes. The solid blue pentagons show the spectro- z sample (Fig. 2), and the open blue pentagons show the photo- z sample (Fig. 3). Both are well fit by a linear relation (dashed line): $\Delta \log_{10} R_{50} = 0.018 - 0.44 \log_{10}(1+z)$. For comparison, the magenta squares show data for disk-dominated galaxies (Sérsic $n < 2.5$) from Trujillo et al. (2006), where the sizes are total galaxy half-light sizes. Error bars are 1σ .

2.3 Evolution of the size - rotation velocity relation

The evolution of the size-velocity (RV) relation has been studied by Bouché et al. (2007) using data from the SINS survey (Förster-Schreiber et al. 2009) at $z \simeq 2$ and from Courteau (1997) at $z = 0$. Using half-width half-maximum (HWHM) sizes interpreted as exponential disk scale lengths, Bouché et al. (2007) found that the RV relation exists at $z = 2$ with the same zero-point as that at $z = 0$.

In this paper we re-determine the zero-point evolution using data from SINS at $z \simeq 2$ adding data from Cresci et al. (2009) to those of Förster-Schreiber et al. (2009). Cresci et al. (2009) determined maximum rotation velocities for 18 galaxies at $z \simeq 2$ from the SINS survey using kinematic modeling of 2D $H\alpha$ velocity fields. Stellar masses were obtained from optical to NIR SED fits assuming Solar metallicity Bruzual & Charlot (2003) stellar population synthesis models with a Chabrier (2003) IMF. Galaxy sizes were measured from $H\alpha$ emission maps using two methods: Cresci et al. (2009) give HWHM sizes, R_{HWHM} , while Förster-Schreiber et al. (2009) give circular half-light sizes, $R_{1/2}$. Both size measurements have been made on the 18 galaxies from Cresci et al. (2009).

The HWHM sizes are obtained from a linear Gaussian fit to the major axis of the $H\alpha$ line intensity maps. According to Bouché et al. (2007), the derived HWHM, once corrected for the observed seeing, corresponds to the expo-

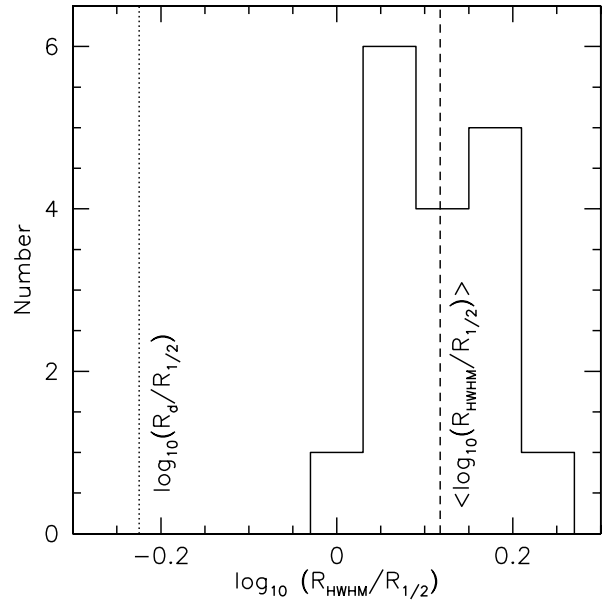


Figure 5. Comparison of $H\alpha$ major-axis HWHM radii, R_{HWHM} , of SINS galaxies from Cresci et al. (2009) and $H\alpha$ half-light radii for the same 18 galaxies from Förster-Schreiber et al. (2009). The HWHM radii are larger on average by 0.12 dex. Bouché et al. (2007) claim that for an exponential distribution, R_{HWHM} equals the exponential scale length, R_d , to within 15%, but then R_{HWHM} should be 0.22 dex smaller than $R_{1/2}$ (see vertical line at left), contrary to what is observed. Thus, either the SINS $H\alpha$ disks are strongly non-exponential and/or the HWHM and half-light radii fundamentally disagree.

ponential scale length, R_d , of the disk. Using simulations of model disks these authors claim that R_d measured this way is likely to be overestimated by no more than 15%. The half-light sizes from Förster-Schreiber et al. (2009) are obtained from the $H\alpha$ curves-of-growth measured in circular apertures, and corrected for seeing.

For an exponential disk, $R_d = 0.60R_{1/2}$, and thus if $R_{\text{HWHM}} \equiv R_d$ then R_{HWHM} should be smaller than $R_{1/2}$ by 0.22 dex, whereas Fig. 5 shows that the opposite is true: the HWHM radii are 0.12 dex larger. The fact that $R_{\text{HWHM}} \simeq 1.3R_{1/2}$ was also noted by Förster-Schreiber et al. (2009). The discrepancy may be somewhat exaggerated, as the half-light radii are measured through circular apertures, not along the major axis. If the galaxies studied by Cresci et al. (2009) were a random sample of galaxies, the median disk inclination angle would be 60 degrees, and thus the circular radii would be too small on average by a factor of $\simeq 1.4$. However, the distribution of disk inclinations of the galaxies in Cresci et al. (2009) appears skewed towards low inclinations: only 3/18 galaxies have inclination greater than 60 degrees. The median inclination is 42 degrees, which implies that the circularization effect is of order 0.07 dex. In what follows we use both size measurements, assuming that R_{HWHM} is equivalent to an exponential scale length and $1.16 \times R_{1/2}$ is equivalent to a major-axis half-light radius. We will let consistency between various data sets determine which, if either, size measurement is more likely to be correct.

Fig. 6 shows the observed evolution of the VMR re-

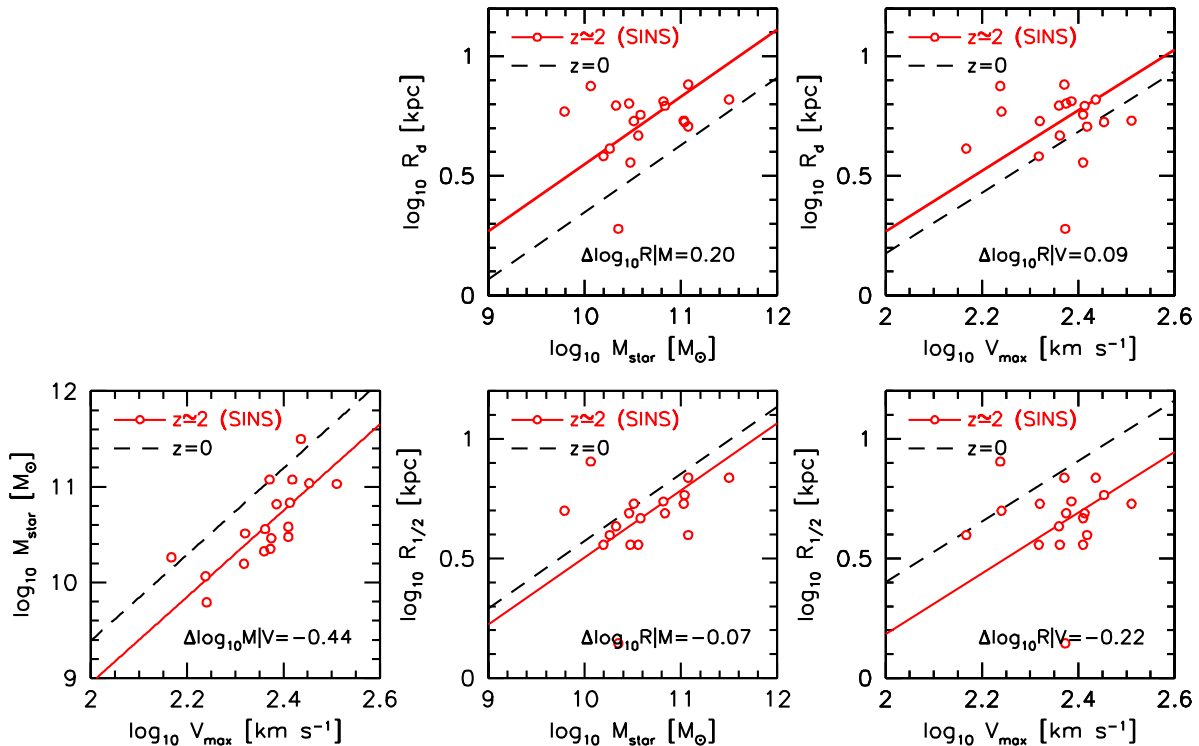


Figure 6. Evolution of the size-stellar mass-rotation velocity relations between redshifts $z = 0$ and $z \simeq 2$. The $z = 0$ relations are from Bell & de Jong (2001) and Dutton et al. (2007), while the $z \simeq 2$ data are from SINS (Cresci et al. 2009; Förster-Schreiber et al. 2009). The stellar masses and maximum rotation velocities are from Cresci et al. (2009). In the upper panels the size is the exponential disk scale length (from Cresci et al. 2009), whereas in the lower panels it is the half-light radius (from Förster-Schreiber et al. 2009). These two size measurements give different, and inconsistent, results for the evolution of disk-galaxy sizes.

lations from $z \simeq 2$ to $z \simeq 0$. The SINS data at $z \simeq 2$ are shown with circles. Two versions of radii are shown: HWHM H α radii by Cresci et al. (2009) (upper panels) and (de-circularized) half-light H α radii by Förster-Schreiber et al. (2009) (lower panels). The redshift $z = 0$ relations are shown as dashed lines and are obtained as follows. We use the $M_{\text{star}} - V_{\text{max}}$ relation from Bell & de Jong (2001) derived from K -band luminosities using a mass dependent extinction correction, subtracting 0.1 dex from the stellar masses to correspond to a Chabrier (2003) IMF, and using a bisector fit:

$$\log_{10} \frac{M_{\text{star}}}{[10^{10} M_{\odot}]} = -0.61 + 4.51 \log_{10} \frac{V_{\text{max}}}{[100 \text{ km s}^{-1}]} \quad (6)$$

We note that the velocity used by Bell & de Jong (2001) is not V_{max} , but actually V_{flat} , the velocity in the flat outer part of the rotation curve. However, as shown by Dutton et al. (2010b) the TF relation derived using V_{max} for these galaxies is identical to the one derived using V_{flat} .

We use the local I -band disk scale length-stellar mass relation from Dutton et al. (2007) which used an orthogonal fit:

$$\log_{10} \frac{R_{d,I}}{[\text{kpc}]} = 0.348 + 0.281 \log_{10} \frac{M_{\text{star}}}{[10^{10} M_{\odot}]}, \quad (7)$$

where we have adopted stellar masses from Bell et al. (2003) -0.1 dex. Taking these MV and RM relations, we infer the mean relation between $R_{d,I}$ and V_{max} :

$$\log_{10} \frac{R_{d,I}}{[\text{kpc}]} = 0.177 + 1.267 \log_{10} \frac{V_{\text{max}}}{[100 \text{ km s}^{-1}]} \quad (8)$$

In order to compare with disk half-light radii we use $R_{50,I} = 1.678 R_{d,I}$. For simplicity we use the I -band sizes to compare with the $z \simeq 2$ data. But we note that the evolution would not change significantly, in fact it would be slightly stronger, if we used the V -band RM relation that we derived from the SDSS.

Due to the small numbers of galaxies in the $z \simeq 2$ sample we do not attempt to fit the slopes of the high-redshift relations. Instead we fix the slopes to the $z = 0$ values and measure the median offset of the $z \simeq 2$ galaxies with respect to the $z = 0$ relations. The values of these offsets are given at the bottom of each panel.

The upper right panel shows the disk scale length-maximum rotation velocity relation using the Cresci et al. (2009) SINS data. The $z \simeq 2$ data have a marginally higher zero point (0.09 ± 0.05 dex) compared to the redshift zero data, which is in agreement with the findings of Bouché et al. (2007). Given that the TF relation evolves to lower stellar masses (-0.44 ± 0.08 dex)⁴ at fixed velocity at higher redshifts (lower left panel), this implies that at fixed stellar

⁴ Note that the difference in evolution of 0.05 dex between our result and that of Cresci et al. (2009), who use the same data, is caused by our different normalization of the $z = 0$ relation from Bell & de Jong (2001). In order to convert the stellar masses derived assuming a “diet”-Salpeter IMF of Bell & de Jong (2001)

mass, sizes should be larger at higher redshifts. As is shown in the upper middle panel, this is indeed the case, with sizes larger by 0.20 ± 0.05 dex at $z \simeq 2$ than $z = 0$. The evolution of the $R_d - M_{\text{star}}$ relation from the SINS Cresci et al. (2009) data is thus of opposite sign to that of previous studies (see § 2.2). In particular it is inconsistent with the $z \sim 2$ results from Trujillo et al. (2006) and Williams et al. (2010), who found that disk/star forming galaxies were a factor of $\simeq 2$ smaller at fixed stellar mass.

The lower middle and right panels show the RM and RV relations using the SINS curve-of-growth $H\alpha$ half-light radii from Förster-Schreiber et al. (2009). These panels show that the half-light sizes are *smaller* at a given stellar or maximum rotation velocity, relative to $z = 0$ galaxies. The offset for the RM relation is -0.07 ± 0.05 dex, while for the RV relation it is -0.22 ± 0.06 dex. The evolution in the RM relation is still however, weaker than obtained by Trujillo et al. (2006), who find -0.28 dex. As we discuss below in § 3.3, this remaining difference can be accounted for by the difference between half-light radii measured in $H\alpha$ and those measured in rest-frame I -band light.

3 THEORETICAL EXPECTATIONS

We now compare these observational results to the predictions of various theoretical models.

3.1 Dark matter haloes

The zeroth order prediction for the evolution of the VMR scaling relations of disk galaxies is given by the evolution of the VMR relations of dark matter haloes. This is obtained by assuming that:

- (i) The total mass profile of the galaxy and halo is isothermal;
- (ii) The galaxy mass fraction, $m_{\text{gal}} = M_{\text{gal}}/M_{\text{vir}}$, is a constant and independent of redshift. Here M_{gal} is the galaxy mass (i.e., the sum of stellar mass and cold gas), and M_{vir} is the total mass within the halo virial radius;
- (iii) The galaxy spin parameter, $\lambda_{\text{gal}} = (j_{\text{gal}}/m_{\text{gal}})\lambda$, is a constant and independent of redshift (for a given halo). Here $j_{\text{gal}} = J_{\text{gal}}/J_{\text{vir}}$ is angular momentum fraction, where J_{gal} is the total angular momentum of the galaxy and J_{vir} is the total angular momentum within the virial radius, and the halo spin parameter, λ , is given by

$$\lambda = \frac{J_{\text{vir}}|E|^{1/2}}{GM_{\text{vir}}^{5/2}} = \frac{J_{\text{vir}}/M_{\text{vir}}}{\sqrt{2}R_{\text{vir}}V_{\text{vir}}} f_c^{1/2}. \quad (9)$$

Here R_{vir} is the virial radius, V_{vir} is the circular velocity at the virial radius, E is the halo's energy, and $f_c = 1$. For more general haloes f_c measures the deviation of E from that of a singular isothermal sphere. For an NFW halo $f_c \simeq \frac{2}{3} + (c/21.5)^{0.7}$ (see Mo, Mao, & White 1998), where c is the halo concentration;

- (iv) The galaxy is 100% stars, i.e., there is no cold gas.

into a Chabrier (2003) IMF, which is used at $z \sim 2$, we adopt -0.1 dex, whereas Cresci et al. (2009) adopted -0.15 dex.

We refer to this model as the singular isothermal sphere (SIS) model. Under these assumptions the disk size scales as the size and circular velocity of the halo (e.g., Mo, Mao, & White 1998): $R_{d,\text{SIS}} = \lambda R_{\text{vir}}/\sqrt{2} \propto V_{\text{vir}}$, and the stellar mass scales with the halo mass: $M_{\text{star}} \propto M_{\text{vir}}$.

Assuming the halo is defined by spherical top hat collapse: $M_{\text{vir}} = (4/3)\pi R_{\text{vir}}^3 \Delta_{\text{vir}} \rho_{\text{crit}}$, then the evolution of the MV , RM , and RV relations is given by:

$$\frac{M_{\text{vir}}(z)}{M_{\text{vir},0}} = \left[\frac{V_{\text{vir}}(z)}{V_{\text{vir},0}} \right]^3 \left[\frac{\Delta_{\text{vir}}(z)}{\Delta_{\text{vir},0}} \right]^{-1/2} \left[\frac{H(z)}{H_0} \right]^{-1} \quad (10)$$

$$\frac{R_{\text{vir}}(z)}{R_{\text{vir},0}} = \left[\frac{M_{\text{vir}}(z)}{M_{\text{vir},0}} \right]^{1/3} \left[\frac{\Delta_{\text{vir}}(z)}{\Delta_{\text{vir},0}} \right]^{-1/3} \left[\frac{H(z)}{H_0} \right]^{-2/3} \quad (11)$$

$$\frac{R_{\text{vir}}(z)}{R_{\text{vir},0}} = \left[\frac{V_{\text{vir}}(z)}{V_{\text{vir},0}} \right] \left[\frac{\Delta_{\text{vir}}(z)}{\Delta_{\text{vir},0}} \right]^{-1/2} \left[\frac{H(z)}{H_0} \right]^{-1}. \quad (12)$$

The zero point evolutions are obtained by setting the leading terms on the RHS=1. Thus the evolution is governed by the evolution of the Hubble parameter $H(z)$ and the halo overdensity within the virial radius, $\Delta_{\text{vir}}(z)$. The evolution of the Hubble parameter (in a flat cosmology) is given by

$$H(z) = H_0[\Omega_{\Lambda} + \Omega_{\text{M}}(1+z)^3]^{1/2}. \quad (13)$$

For the evolution of the halo overdensity, $\Delta_{\text{vir}}(z)$, we use the fitting formula from Bryan & Norman (1998): $\Delta_{\text{vir}} = 18\pi^2 + 82x - 39x^2$, where $x = \Omega(z) - 1$ and $\Omega(z)$ is defined as $\Omega_{\text{M}}(1+z)^3 [H(z)/H_0]^{-2}$.

Thus to first order the evolutions are determined by the evolution of the Hubble parameter and to second order by the evolution of the halo overdensity. These predicted evolutions, for a Λ CDM cosmology with $\Omega_{\text{M}} = 0.3$ and $\Omega_{\Lambda} = 0.7$, are shown by the dashed lines in Fig. 7. For the $M_{\text{vir}} - V_{\text{vir}}$ and $R_{\text{vir}} - V_{\text{vir}}$ relations the evolution scales roughly as $(1+z)^{-1.3}$, while for the $R_{\text{vir}} - M_{\text{vir}}$ relation the evolution scales roughly as $(1+z)^{-0.8}$. The observed evolution of the maximum circular velocity - stellar mass - half-light radius relations is given by the colored symbols. For the stellar mass-velocity relation we use data from: Conselice et al. (2005, green triangles); DEEP2 - Kassin et al. (2007, blue pentagons); and SINS - Cresci et al. (2009, red open circle). For the size-stellar mass relation we use data from: Trujillo et al. (2006, magenta squares); SINS - Cresci et al. (2009, red open circle) and Förster-Schreiber et al. (2009, red open square); Williams et al. (2010, green triangles); and DEEP2 - this paper (blue pentagons). For the size-velocity relation we use data from: SINS - Cresci et al. (2009, red open circle) and Förster-Schreiber et al. (2009, red open square). These observations are described in more detail in §2. As has been noted by previous authors, the observed evolution of all three VMR relations is weaker than this simple prediction from dark matter haloes.

The SIS model makes a number of simplifying assumptions that are likely to be incorrect. Firstly, total mass density profiles are not expected to be globally isothermal. Dark matter haloes in cosmological simulations have $V_{\text{max}} > V_{\text{vir}}$ (e.g., Bullock et al. 2001a). In addition, the contribution of the baryons to the inner potential can increase the observed V_{max} even further.

Using the models of Mo, Mao, & White (1998), Somerville et al. (2008) showed that including the expected

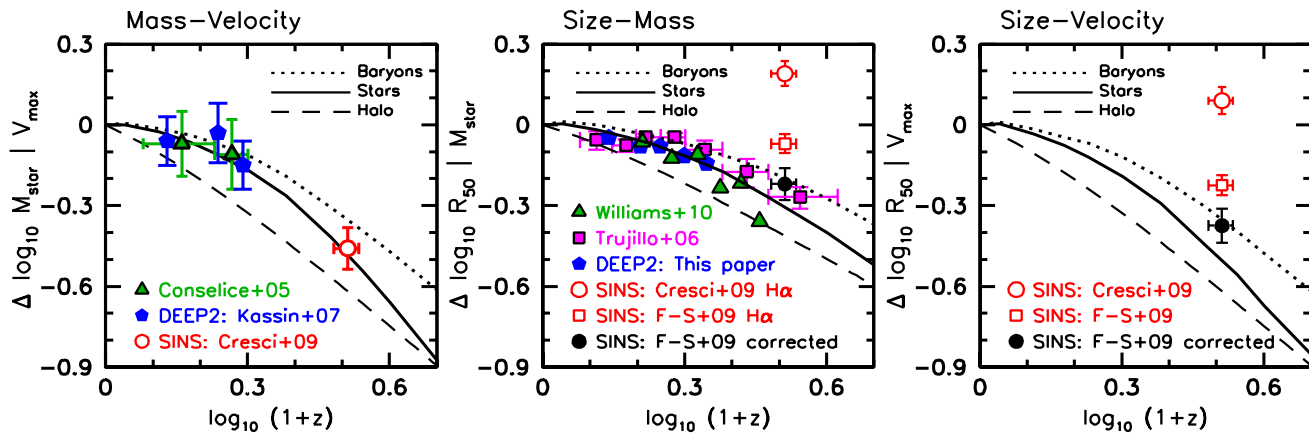


Figure 7. Evolution of the circular velocity - mass - size relations in observations and models. The data are given by colored symbols, as indicated, and are described in §2. The evolution of the stellar relations ($V_{\max} - M_{\text{star}} - R_{50V}$) in a Λ CDM disk galaxy evolution model are given by solid lines. The models and data are consistent, with the exception of the sizes of galaxies in the SINS survey as measured by Cresci et al. (2009), which appear to be a factor of $\simeq 3$ too large (red open circles). This discrepancy is partially removed when using H α half-light sizes from Förster-Schreiber et al. (2009) (red open squares), and fully removed after correcting these sizes from H α to rest-frame I -band (black solid circles). For comparison, the evolution of the baryonic ($V_{\max} - M_{\text{gal}} - R_{\text{gal}}$) and halo virial ($V_{\text{vir}} - M_{\text{vir}} - R_{\text{vir}}$) relations are given by the dotted and dashed lines, respectively. The evolution of the theoretical virial, baryonic, and stellar relations are given in Table 3.

evolution in dark halo concentrations, as well as the contribution of baryons to the potential, results in weaker evolution than predicted by the SIS model. However, Somerville et al. (2008) make the assumption that disks have no gas, and thus, that the stellar mass is equal to the baryonic mass and the V -band half-light radius is equal to the baryonic half-mass radius. In order to determine whether the stellar relations evolve differently from the baryonic relations, one needs to follow the evolution of stellar and gas disks in a self-consistent way. This requires realistic cosmological simulations with gas or semi-analytic models (SAMs). Here we use the latter.

3.2 Disk galaxy semi-analytic model

In order to calculate the evolution of stellar disks as opposed to baryonic disks, we use the disk galaxy SAM of Dutton & van den Bosch (2009). This model consists of disks that grow inside evolving NFW haloes (Navarro, Frenk, & White 1997), with structure determined from cosmological N-body simulations (Bullock et al. 2001a; Macciò, Dutton & van den Bosch 2008), a median spin parameter λ , which is independent of redshift, and halo specific angular momentum distributions from Sharma & Steinmetz (2005), which are specified by a parameter, α . The cumulative distribution of specific angular momentum $P(< s)$, where s is the specific angular momentum in units of the total specific angular momentum, is given by

$$P(< s) = \gamma(\alpha, \alpha s), \quad (14)$$

where γ is the incomplete gamma function. In this model, disks are not formally exponential, but the stellar disks can often be well described by an exponential profile over several scale lengths (Dutton 2009).

To build a model as close as possible to the SIS model, we maintain assumptions (ii) and (iii) from above. As in

Somerville et al. (2008), the baryonic disk is in dynamical equilibrium inside an NFW halo which evolves with redshift according to cosmological simulations (Bullock et al. 2001a). The key difference is that we do not make assumption (iv), i.e., that the disk is 100% stars. In our model, the evolution of the stellar and gas disks (and hence stellar and gas mass) is governed by the radial variation of star formation, gas recycling, and accretion. The stellar mass is thus always less than the baryonic mass, and the stellar disk is usually smaller in radius than the baryonic disk. Because our model follows stellar populations as a function of radius, we calculate the sizes of model galaxies in optical to NIR light, as well as stellar and baryonic mass. This allows us to test whether the sizes measured in different pass-bands and masses are equivalent.

An additional difference between our models and those of Somerville et al. (2008) is halo contraction. Somerville et al. (2008) assumed that haloes contract according to the Blumenthal et al. (1986) adiabatic contraction model. In our model, we leave the haloes uncontracted, as models with dark halo contraction (and standard IMFs) are unable to reproduce the zero points of the VMR relations (Dutton et al. 2007). There are a variety of astrophysical processes that could reverse the expected effect of halo contraction. These include dynamical friction from massive clumps of baryons (e.g., El-Zant, Shlosman & Hoffman 2001; Mo & Mao 2004; Elmegreen et al. 2008; Jardel & Sellwood 2009), dynamical friction due to bars (e.g., Weinberg & Katz 2002; Sellwood 2008), and rapid mass outflows due to supernova feedback (e.g., Mo & Mao 2004; Read & Gilmore 2005; Governato et al. 2010), so our choice of not including adiabatic contraction is at least physically plausible as well as being empirically motivated. As we will see from the success of our models in matching the evolution of the VMR relations, halo contraction is also not required in order to reproduce the observed evolution of the VMR relations.

Table 3. Evolution of the stellar, baryonic, and virial velocity-mass-size relations of our disk-galaxy evolution model, with $m_{\text{gal}} = 0.04$ and $\lambda = 0.035$, relative to redshift $z = 0$ as shown in Fig. 7.

z	$\log_{10}(1+z)$	$\Delta \log_{10} M_{\text{star}} V_{\text{max}}$	$\Delta \log_{10} M_{\text{gal}} V_{\text{max}}$	$\Delta \log_{10} M_{\text{vir}} V_{\text{vir}}$
0.00	0.000	0.000	0.000	0.000
0.10	0.041	-0.001	0.006	-0.035
0.30	0.114	-0.027	-0.014	-0.106
0.51	0.179	-0.065	-0.039	-0.177
0.70	0.230	-0.105	-0.066	-0.238
1.01	0.303	-0.171	-0.115	-0.327
1.41	0.382	-0.264	-0.190	-0.435
2.00	0.477	-0.418	-0.307	-0.568
2.50	0.544	-0.543	-0.394	-0.665
3.00	0.602	-0.661	-0.472	-0.749
4.00	0.699	-0.872	-0.610	-0.892

z	$\log_{10}(1+z)$	$\Delta \log_{10} R_{50V} M_{\text{star}}$	$\Delta \log_{10} R_{50\text{gal}} M_{\text{gal}}$	$\Delta \log_{10} R_{\text{vir}} M_{\text{vir}}$
0.00	0.000	0.000	0.000	0.000
0.10	0.041	0.003	0.012	-0.024
0.30	0.114	-0.019	-0.001	-0.071
0.51	0.179	-0.046	-0.022	-0.118
0.70	0.230	-0.071	-0.042	-0.159
1.01	0.303	-0.116	-0.071	-0.218
1.41	0.382	-0.175	-0.112	-0.290
2.00	0.477	-0.270	-0.170	-0.379
2.50	0.544	-0.339	-0.224	-0.443
3.00	0.602	-0.402	-0.276	-0.500
4.00	0.699	-0.519	-0.368	-0.595

z	$\log_{10}(1+z)$	$\Delta \log_{10} R_{50V} V_{\text{max}}$	$\Delta \log_{10} R_{50\text{gal}} V_{\text{max}}$	$\Delta \log_{10} R_{\text{vir}} V_{\text{vir}}$
0.00	0.000	0.000	0.000	0.000
0.10	0.041	0.003	0.010	-0.035
0.30	0.114	-0.035	-0.016	-0.106
0.51	0.179	-0.077	-0.046	-0.177
0.70	0.230	-0.120	-0.069	-0.238
1.01	0.303	-0.192	-0.121	-0.327
1.41	0.382	-0.291	-0.197	-0.435
2.00	0.477	-0.448	-0.306	-0.568
2.50	0.544	-0.557	-0.395	-0.665
3.00	0.602	-0.672	-0.479	-0.749
4.00	0.699	-0.850	-0.614	-0.892

In the model used here, we adopt a cosmology with $(\Omega_M, \Omega_\Lambda, h, \sigma_8, n) = (0.3, 0.7, 0.7, 0.8, 1.0)$, which is close to that of the WMAP 5th year results (Dunkley et al. 2009). We adopt a galaxy mass fraction of $m_{\text{gal}} = (M_{\text{star}} + M_{\text{gas}})/M_{\text{vir}} = 0.04$, a median spin parameter of $\bar{\lambda}_{\text{gal}} = \bar{\lambda} = 0.035$, and a median angular momentum shape parameter of $\bar{\alpha} = 0.9$. These parameters are motivated by observations of m_{gal} (Hoekstra et al. 2005; Dutton et al. 2010b) and theoretical predictions for λ (Bullock et al. 2001b; Macciò et al. 2007) and α (Sharma & Steinmetz 2005). They also result in models that roughly reproduce the observed VMR relations at $z = 0$ (Fig. 8). However, this model does not exactly reproduce the slopes of the local VMR relations. Doing so requires either m_{gal} or λ_{gal} to vary with halo mass (e.g., Shen et al. 2003; Dutton et al. 2007).

We generate a Monte Carlo sample of 2000 galaxies with halo masses between $M_{\text{vir}} = 10^{10.3} - 10^{13.5} h^{-1} M_\odot$, log-normal scatter in spin parameter of $\sigma_{\ln \lambda} = 0.5$ (Bullock et al. 2001b), log-normal scatter in halo angular mo-

mentum profile of $\sigma_{\ln \alpha} = 0.25$ (Sharma & Steinmetz 2005), and log-normal scatter in halo concentration of $\sigma_{\ln c} = 0.25$ (Macciò et al. 2008). We determine the evolution of the zero points of the model VMR relations by fitting the MV and RV relations for $2.1 \leq \log_{10}(V_{\text{max}}/[\text{km s}^{-1}]) \leq 2.5$ and the RM relations for $9.0 \leq \log_{10}(M_{\text{star}}/[M_\odot]) \leq 11.0$. We then calculate the evolution at $\log_{10}(V_{\text{max}}/[\text{km s}^{-1}]) = 2.3$ and $\log_{10}(M_{\text{star}}/[M_\odot]) = 10.5$.

The solid lines in Fig. 7 show evolution in the zero points of the $V_{\text{max}} - M_{\text{star}} - R_{50V}$ (i.e., maximum circular velocity, stellar mass, V -band half-light radius) relations of this model from redshifts $z = 4$ to $z = 0$. These relations show weaker evolution than the virial relations (dashed lines), but stronger evolution than the baryonic relations (dotted lines). The evolution of the theoretical virial, baryonic, and stellar relations are given in Table 3.

One interpretation of the weak evolution of the galaxy scaling relations since $z \sim 1$ is that individual galaxies also evolve weakly since $z \sim 1$. However, disk-galaxies were form-

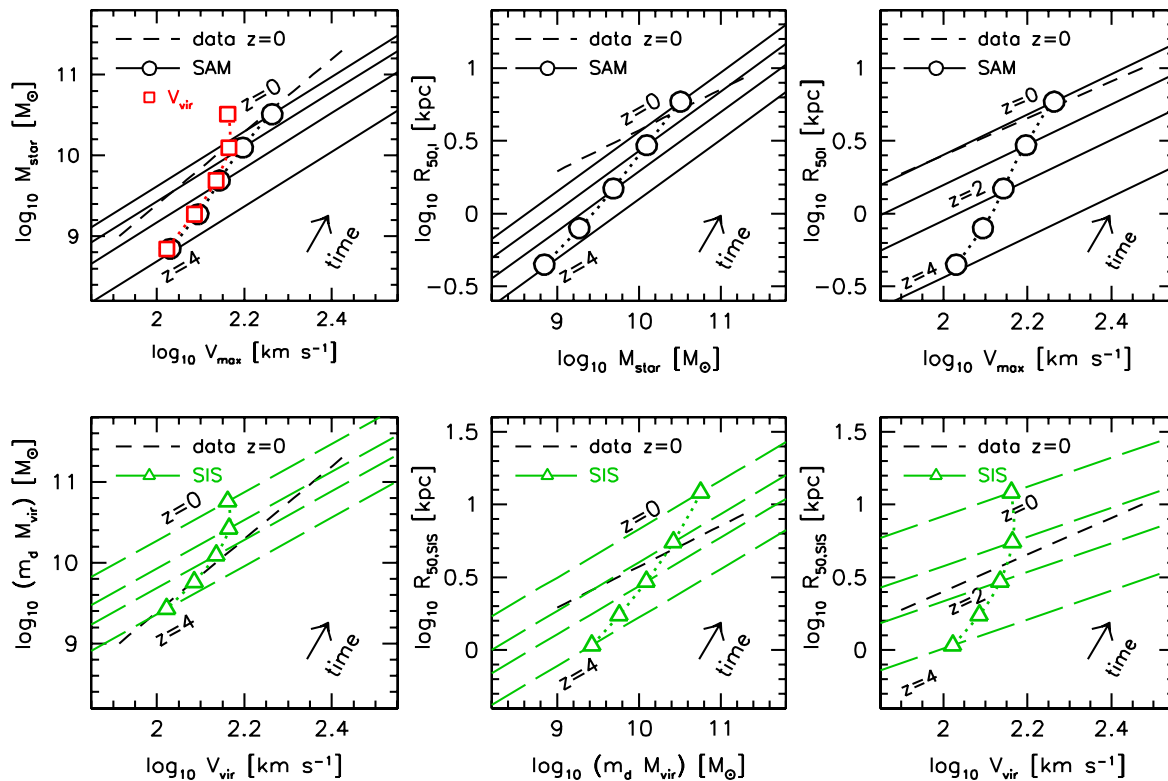


Figure 8. Evolution of the maximum circular velocity - stellar mass - half-light radius relations in our Λ CDM disk-galaxy evolution model. Power-law fits to the $(V_{\max} - M_{\text{star}} - R_{50I})$ relations at redshifts $z = 4, 2, 1, 0$ are given by solid black lines. The $z = 0$ observations are given by short-dashed black lines. The symbols show the evolution of an individual galaxy with redshift $z = 0$ halo virial mass of $M_{\text{vir}} = 10^{12} h^{-1} M_{\odot}$ at $z = 4, 3, 2, 1, 0$ (from lower left to top right). The black circles show the evolution of $V_{\max} - M_{\text{star}} - R_{50I}$. There is substantial growth in these three quantities, in a roughly power-law from $z = 4$ to $z = 0$ (black dotted lines). The green triangles show the evolution of the SIS model, which is identical to the evolution of the halo virial quantities. To facilitate comparison between the galaxy and virial properties, the red squares show $M_{\text{star}} - V_{\text{vir}}$ and $M_{\text{star}} - R_{\text{d,SIS}}$. The weak evolution of galaxy scaling relations since $z \sim 1$ is due to the fact that individual galaxies grow roughly along the scaling relations.

ing stars at much higher rates in the past (e.g., Noeske et al. 2007a), and thus stellar masses are expected to grow significantly since $z \sim 1$. Simple models for the evolution of the star formation rate-stellar mass relation suggest that galaxies with present day stellar masses of $3 \times 10^{10} M_{\odot}$ had stellar masses a factor of $\simeq 2.5$ lower at $z = 1$ (Noeske et al. 2007b). This amount of evolution in stellar masses is consistent with that predicted by our model. Fig. 8 shows the evolution of a galaxy with present day stellar mass of $3 \times 10^{10} M_{\odot}$. Since $z = 1$ its stellar mass has increased by a factor of $\simeq 2.5$, its half-light size has increased by a factor of $\simeq 2$, and its maximum circular velocity has increased by a factor of $\simeq 1.15$. In terms of samples of galaxies, the evolution since $z = 1$ is just a factor of $\simeq 1.5$ increase in stellar masses, at fixed V_{\max} , and a factor of $\simeq 1.3$ increase disk size, at fixed stellar mass. Thus, the scaling relations between properties of galaxies ($V_{\max} - M_{\text{star}} - R_{50I}$) evolve only weakly since $z \sim 1$ because individual galaxies evolve roughly *along* the scaling relations. Similar theoretically based conclusions have been made previously for the stellar mass - velocity relation (Portinari & Sommer-Larsen 2007) and the size-stellar mass relation (Firmani & Avila-Reese 2009).

The differences between the evolution of the baryonic and virial MV relations (dotted vs. dashed lines in Fig. 7) are due solely to evolution in the ratio between V_{\max} and V_{vir} and not due to an evolution in the ratio between the baryonic mass and virial mass, m_{gal} , which is fixed to a constant in this model. The ratio between V_{\max} and V_{vir} increases towards lower redshift due to higher concentrations in lower redshift haloes. This results in less evolution in V_{\max} than V_{vir} at fixed M_{gal} or M_{vir} , and hence less evolution in M_{gal} or M_{vir} at fixed V_{\max} than at fixed V_{vir} . The evolution of V_{\max} and V_{vir} for an individual galaxy with redshift $z = 0$ virial mass of $M_{\text{vir}} = 10^{12} h^{-1} M_{\odot}$ and median halo parameters is shown in the left panels of Fig. 8. This shows that for high redshifts ($z \gtrsim 2$) $V_{\max} \simeq V_{\text{vir}}$, but for low redshifts ($z \lesssim 1$) V_{vir} remains constant while V_{\max} continues to increase. At redshift $z = 0$, $V_{\max} \simeq 1.3V_{\text{vir}}$, which is consistent with recent measurements (Dutton et al. 2010b). The lower middle panel of Fig. 8 shows that R_{vir} and M_{vir} both continue to increase at low redshifts. The reason V_{vir} remains roughly constant while R_{vir} and M_{vir} increase is due to a trade off between the addition of new mass (which increases V_{vir}) and the increase of the virial radius (which decreases V_{vir} because the circular velocity of the NFW profile declines at large radius).

Since the baryonic mass fraction we adopt is only $\simeq 25\%$ of the universal baryon fraction, it is certainly plausible that the mechanisms responsible for making galaxy formation inefficient result in m_{gal} varying with redshift. However, to first order, variation in m_{gal} moves galaxies along the VM relation (e.g., Navarro & Steinmetz 2000; Dutton et al. 2007), and thus we expect that large changes in m_{gal} with redshift would be needed in order to significantly change the evolution from that predicted by our constant m_{gal} model.

The differences between the evolution of the baryonic and virial RM relations in Fig. 7 are caused by evolution in the ratio between baryonic and virial sizes (because the baryon mass fraction is a constant), which are roughly given by: $R_{50\text{gal}}/R_{\text{vir}} \propto \lambda_{\text{gal}}(V_{\text{vir}}/V_{\text{max}})f_c^{-1/2}$. Thus as with the MV relations, the differences between the baryonic and virial RM relations are driven by the evolution in $V_{\text{max}}/V_{\text{vir}}$. Unlike the VM relation, the baryonic RM relation is sensitive to the adopted baryon mass fraction (Dutton et al. 2007). Thus if m_{gal} decreases (or increases) with increasing redshift, this will result in weaker (or stronger) evolution in the baryonic RM relation.

The differences between the evolution of the baryonic and virial RV relations are determined by evolution in both $R_{50\text{gal}}/R_{\text{vir}}$ and $V_{\text{max}}/V_{\text{vir}}$. Evolution in the size ratio accounts of $\simeq 2/3$ of the evolution difference, while evolution in the velocity ratio accounts for the remaining $\simeq 1/3$. As with the RM relation, the RV relation is sensitive to the galaxy mass fraction, with a similar sign dependence.

The differences between the stellar and baryonic MV relations in Fig. 7 can be understood as a result of the higher cold gas fractions at higher redshifts in our model. We note that the evolution in the cold gas fractions in our model is relatively modest, with a factor of $\lesssim 2$ increase in gas masses at fixed stellar mass between redshift $z = 0$ and $z = 2$. As shown by Dutton, van den Bosch & Dekel (2010a), more general models (including cooling and outflows) also predict weak evolution in cold gas fractions, but strong evolution in molecular gas fractions. Both of these predictions are consistent with recent observations (e.g., Erb et al. 2006; Daddi et al. 2010; Tacconi et al. 2010; Puech et al. 2010).

Higher cold gas fractions also contribute to different evolution in the stellar and baryonic RV and RM relations. But there are also contributions from differences between sizes in stellar mass and sizes in optical light, which are a consequence of the inside-out nature of stellar disk growth in our models. These differences are discussed in more detail below.

3.3 Reconciling SINS sizes with other observations

Our model nicely reproduces the observed zero point evolution of the stellar mass Tully-Fisher ($M_{\text{star}} - V_{\text{max}}$) and size-stellar mass relations from $z = 2.2$ to $z = 0$ (Fig. 7). The model also predicts a factor of $\simeq 3$ evolution in the zero point of the optical half-light size-velocity relation ($R_{50V} - V_{\text{max}}$) over this redshift range (solid black line in the right panel of Fig. 7). However, the $R_{\text{d}} - V_{\text{max}}$ data from SINS (using disk scale lengths from Cresci et al. 2009) indicate weak evolution in the opposite direction from $z = 2.2$ to $z = 0$ (red open cir-

cle in the right panel of Fig. 7). Recall that we have derived the evolution of the $R_{\text{d}} - V_{\text{max}}$ relation by comparing with the I -band $R_{\text{d}} - V_{\text{max}}$ relation at $z = 0$ (see § 2.3). Since the Cresci et al. (2009) data set also implies that higher redshift galaxies are larger at fixed stellar mass (red open circle in the middle panel of Fig. 7), this obviously means that the evolution of the scaling relations between different data sets are inconsistent. The offset between the observed RM evolution from Trujillo et al. (2006) and the Cresci et al. (2009) SINS data is also a factor of $\simeq 3$. Thus if the Cresci et al. (2009) disk scale lengths of the SINS galaxies could be reduced by a factor of $\simeq 3$, then all of the data sets would be consistent. Furthermore, the data would be consistent with our simple, but cosmologically motivated, model for disk-galaxy evolution.

As discussed in §2.3, there are two size measurements now available for SINS galaxies, both based on $H\alpha$ imaging: major axis HWHM sizes by Cresci et al. (2009) (which have been interpreted as being equivalent to disk scale lengths), and circular half-light radii by Förster-Schreiber et al. (2009). In §2.3 we calculated the evolution of the SINS data at $z \simeq 2.2$ relative to the I -band RM and RV relations at $z = 0$. We found that the two size measurements resulted in very different amounts of evolution, with the half-light sizes giving a factor of $\simeq 2$ smaller sizes at higher redshift. Thus using the SINS half-light sizes by Förster-Schreiber et al. (2009) (red open squares in Fig. 7) removes most of the discrepancy that exists when using the Cresci et al. (2009) HWHM sizes interpreted as disk scale lengths.

However, there is still a small discrepancy at the 0.2 dex level between the evolution of the SINS half-light sizes with those from Trujillo et al. (2006), Williams et al. (2010), and our models. Below we discuss whether this difference can be explained by the difference between sizes measured in $H\alpha$ compared to rest-frame I -band light. Since the SINS survey is not a volume limited sample of galaxies at high-redshift, and at least some of the SINS sample was selected on the basis of disk morphology with spatially resolved velocity gradients, another possibility is that a selection bias against small galaxies exists in the SINS survey.

3.4 The relation between sizes in $H\alpha$ vs. rest-frame optical light

How well do galaxy sizes measured in $H\alpha$ trace those measured in rest-frame optical stellar light? We now address this question using the disk SAM discussed in § 3.2. To make our comparison, we assume that $H\alpha$ is a reliable tracer of recent star formation, where recent star formation in our models is the star formation within the last time step (i.e., $\simeq 30$ to 100 Myr). For simplicity, we also ignore the effects of dust, which may modify the relation between sizes measured in $H\alpha$ and optical light. Fig. 9 shows the results where we compare the half-mass radii of recent star formation, R_{SF} , in our disk formation model, to the half-light radii in the near-UV to near-IR pass bands.

We find that the half-mass radius of the recent star formation is on average a factor of $\simeq 2$ larger than the half-mass radius of the total stellar mass. This is a signature of the “inside-out” nature of stellar disk growth in our models. The inside-out growth is due to a combination of two factors: (1) For an individual galaxy the baryonic disk grows

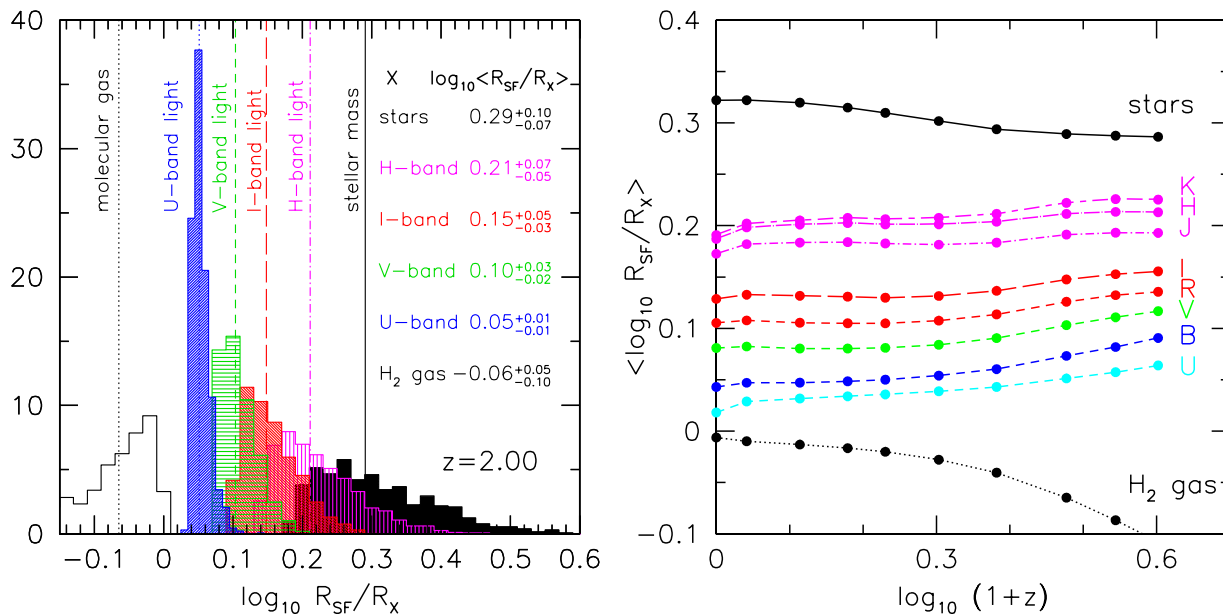


Figure 9. Ratios of galaxy sizes (half-mass or half-light) in recently formed stars (within the last 100Myr), R_{SF} , to sizes in various rest-frame optical-near-infrared pass bands, R_X , at redshift $z = 2$ (left) and as a function of redshift (right) in a cosmological disk galaxy evolution model. The numbers show the median ratio together with the 16th and 84th percentiles of the distribution. The half-mass radius of the recently formed stars is, on average, a factor of ≈ 2 larger than the half-mass radius of the total stellar mass. This reflects the fact that stellar disks are growing inside out in this model. These differences persist, but are not as big, when comparing R_{SF} to optical half-light radii. At $z = 2$ the rest-frame *I*-band half-light sizes are ≈ 0.15 dex smaller than star formation sizes. These ratios evolve only weakly with redshift in our model.

with time due to an increase in the specific angular momentum. This is cosmological inside-out growth; (2) The density dependence of the star formation law (star formation is less efficient at lower gas densities). This is star formation induced inside-out growth.

Using cosmological hydrodynamical simulations of galaxies at redshift $z \approx 2$ Sales et al. (2009) found a similar factor of ≈ 1.8 difference between the half-mass sizes of the dense (star forming) gas and the half-mass sizes of the stellar mass. However, as we go from stellar mass sizes to NIR sizes to optical sizes, the differences with respect to the star formation sizes decrease. In terms of optical half-light radii, the star formation size is just 0.1 dex higher than *V*-band sizes and 0.15 dex higher than *I*-band sizes at $z = 2$. Thus Fig. 9 suggests that the differences between $H\alpha$ and optical sizes by themselves are unlikely to explain the full factor of 3 discrepancy between the SINS disk scale lengths and the other observations shown in Fig. 7. But, as shown by the solid red circles, these are of the right magnitude to fully remove the lingering small discrepancy between the Förster-Schreiber et al. (2009) half-light radii and the Trujillo et al. (2006) data and our models.

To summarize, we have shown that the radii of SINS galaxies can plausibly be reconciled with other observational data and with theoretical models provided proper radii are used (half-light radii, not HWHM) and provided a small correction is applied to convert $H\alpha$ radii to optical radii. Ideally this agreement should be verified directly with sizes measured in rest-frame optical light, and preferably using the same techniques and definitions as used at lower redshifts. It would also be desirable to test this concordance by mea-

suring the evolution of the *VMR* relations at redshifts $z \gtrsim 1$ using larger samples of galaxies and over a wider range of masses than current studies. The measurement of rest-frame optical sizes of galaxies at $z \sim 2$ is currently possible with *H*-band imaging with *HST*, and *H* & *K*-band imaging with adaptive optics from the ground.

The right panel of Fig. 9 predicts that not much evolution is expected in the size ratios between different pass-bands. Thus as a test of how realistic the size ratios of our models are at high redshift, we can compare them to observations of size ratios at low redshift. Fig. 9 shows that at redshift $z = 0$ the sizes in the *B*-band should be larger than those in the *V*, *R* and *H*-bands by 0.037, 0.061, and 0.145 dex, respectively. This is consistent with observations of nearby spiral galaxies by MacArthur, Courteau & Holtzman (2003) who find differences of 0.029, 0.061, and 0.127 dex. While this does not prove that our model predicts the correct size ratios for $z = 2$ galaxies, it does provide indirect support.

Another prediction of the model is that sizes in molecular gas should be only slightly larger than sizes in $H\alpha$ or UV light. This is a consequence of the almost linear relation between star formation rate surface density and molecular gas surface density in our model (See Fig. A1, Dutton et al. 2010a). At higher molecular gas densities the slope of the star formation law in our model is steeper than unity, with an asymptotic value of 1.4, in agreement with the standard Kennicutt-Schmidt relation (Kennicutt 1998). Since molecular gas disks are predicted to be higher density at higher redshifts, this results in a slight evolution in the ratio between molecular gas sizes and star formation rate sizes

Table 4. Evolution of the TF relation in optical to near-IR luminosities from disk-galaxy evolution model relative to redshift $z = 0$ as shown in Fig. 10.

z	$\log_{10}(1+z)$	$\Delta \log_{10} L_B V_{\max}$	$\Delta \log_{10} L_V V_{\max}$	$\Delta \log_{10} L_J V_{\max}$	$\Delta \log_{10} L_K V_{\max}$	$\Delta \log_{10} L_K V_{\max}$
0.00	0.000	0.000	0.000	0.000	0.000	0.000
0.10	0.041	0.123	0.068	0.022	0.001	-0.005
0.30	0.114	0.236	0.151	0.076	0.034	0.021
0.51	0.179	0.296	0.200	0.107	0.051	0.034
0.70	0.230	0.329	0.225	0.123	0.060	0.038
1.01	0.303	0.357	0.250	0.137	0.060	0.036
1.41	0.382	0.374	0.263	0.139	0.048	0.018
2.00	0.477	0.353	0.234	0.094	-0.010	-0.051
2.50	0.544	0.319	0.191	0.043	-0.070	-0.118
3.00	0.602	0.279	0.143	-0.016	-0.132	-0.186
4.00	0.699	0.192	0.047	-0.123	-0.245	-0.311

in our model (right panel, Fig. 9). The similarity between molecular gas sizes and UV sizes has already been observed for a handful of star forming galaxies at redshift $z \sim 1.5$ (Daddi et al. 2010), which provides further support for our model.

3.5 The evolution of the Tully-Fisher relation in optical to near-IR luminosities

The evolution of our model Tully-Fisher relations in optical to near-IR luminosities is shown in Fig. 10 and in Table 4. Contrary to the stellar and baryonic TF relations, which show a *decrease* in mass at fixed circular velocity (solid and dotted lines), the luminosity TF relations show an *increase* in luminosity at fixed circular velocity between today and redshift $z \sim 1$. Luminosities in bluer pass-bands show stronger evolution than redder pass-bands. In the B -band, the evolution is 0.36 dex (or 0.9 magnitudes) since $z = 1$, while in the K -band, the evolution is just 0.04 dex (or 0.1 magnitudes) since $z = 1$. A similar theoretical prediction of 0.85 mag for the evolution of the B -band TF relation since $z = 1$ has been shown by Portinari & Sommer-Larsen (2007) using cosmological hydrodynamical simulations. Using a semi-analytic model Firmani & Avila-Reese (2003) find differences between the evolution of the B -band and H -band TF relations which are qualitatively similar to what we find in our models, though in detail there are differences in the absolute evolution.

Most observations find no or weak evolution in the J - and K -band TF relations since $z \sim 1$ (Conselice et al. 2005; Weiner et al. 2006b; Flores et al. 2006; Fernández Lorenzo et al. 2010), which is in good agreement with our model (but see Puech et al. (2008) who find 0.6 magnitudes of brightening between $z \sim 0.6$ and $z = 0$). For the B -band TF relation, a wide range of evolution has been reported, but almost all studies find a brightening in B -band luminosities at higher redshifts (e.g., Vogt et al. 1996,1997; Simard & Pritchett 1998; Ziegler et al. 2002; Böhm et al. 2004; Bamford et al. 2005,2006; Weiner et al. 2006b; Chiu et al. 2007; Fernández Lorenzo et al. 2010). Most studies are consistent with a brightening of 1 ± 0.5 magnitudes from $z = 0$ to $z \sim 1$, and thus in agreement with our model.

Finally, we note that no evolution in the J - or K -band TF relation does not imply no evolution in the stellar mass

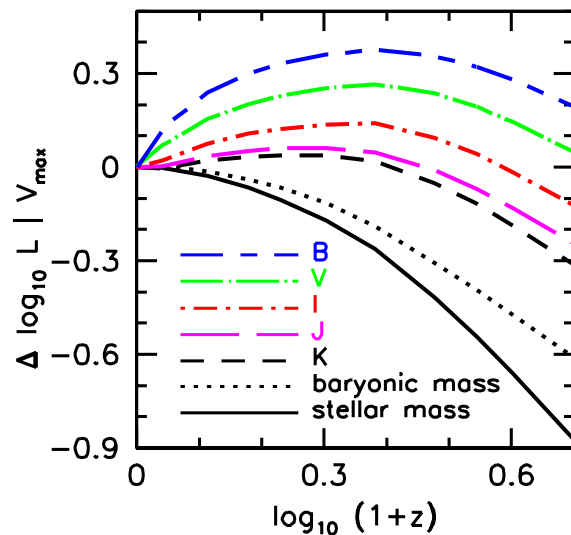


Figure 10. Evolution of the Tully-Fisher relation using luminosities measured in rest-frame optical to near-IR pass bands in our disk-galaxy semi-analytic model. At fixed circular velocity, luminosities increase out to redshift $z \simeq 1.5$, with stronger evolution in bluer passbands than the near-IR. For comparison, the evolution of the stellar and baryonic Tully-Fisher relations are shown with solid and dotted lines, respectively, which are the same as those in the left panel of Fig. 7.

TF relation. In our model the stellar masses at fixed velocity decrease towards higher redshifts, but the light-to-mass ratios increase monotonically towards higher redshifts (because the stellar populations are progressively younger). The net effect is very weak evolution in J - and K -band TF relations between $z \sim 2$ and $z = 0$.

4 SUMMARY

We study the evolution in the zero points of the relations between maximum rotation velocity, V , stellar mass, M , and rest-frame optical disk size, R , of disk-galaxies in the context of Λ CDM based galaxy formation models.

Using data from the DEEP2 survey to measure the

evolution of the RM relation since $z = 1.2$, together with published results from Conselice et al. (2005), Trujillo et al. (2006), Kassin et al. (2007), and the SINS survey (Cresci et al. 2009; Förster-Schreiber et al. 2009), we show that there is a consistent observational picture, with one exception, for the evolution of the VMR relations from redshifts $z \simeq 2.2$ to $z \simeq 0$. The exception is that the $H\alpha$ exponential disk scale lengths of galaxies from the SINS survey measured by Cresci et al. (2009), appear to be a factor of $\simeq 3$ higher at fixed M than found by other observations. This apparent discrepancy can be traced to two factors.

Firstly, Bouché et al. (2007) and Cresci et al. (2009) measure HWHM (half-width half-max) sizes and interpret these as exponential disk scale lengths. However, the $H\alpha$ half-light radii from Förster-Schreiber et al. (2009) of the same galaxies do not support this interpretation. Instead, they suggest that the HWHM overestimates the disk scale length by a factor of $\simeq 2$.

Secondly, using a Λ CDM based disk galaxy formation model (Dutton & van den Bosch 2009) we show that disk-galaxies at redshifts $z = 0-3$ are expected to have half-mass radii of recently formed stars, R_{SF} , a factor of $\simeq 2$ higher than the half-mass radius of the total stellar mass, R_{star} . This is a direct consequence of inside out disk growth. In terms of optical half-light radii, our models predict that, $R_{SF} \simeq 1.4R_I \simeq 1.25R_V$ with little dependence on redshift.

Additionally, since the SINS survey is not a volume limited sample of galaxies at high-redshift, and at least some of the SINS sample was selected on the basis of disk morphology with spatially resolved velocity gradients, another possibility (which we do not invoke here) is that a selection bias against small galaxies exists in the SINS survey. In order to rule-out this possibility the size-mass relation of SINS galaxies needs to be compared to that of a volume limited control sample, with the same methods used to derive sizes and masses.

We further show that the observed evolution of the VMR relations is consistent with a simple Λ CDM-based model of disks growing inside evolving NFW dark-matter haloes. This model adopts a constant disk-to-halo mass fraction of $m_d = 0.04$, and a median spin parameter of $\lambda = 0.035$, independent of redshift. The galaxy mass fraction is consistent with observations at low redshifts (Hoekstra et al. 2005; Dutton et al. 2010b), and the spin parameter is consistent with expectations from cosmological simulations (e.g., Bullock et al. 2001b; Macciò et al. 2007). While our model is certainly an over-simplification of disk-galaxy evolution, it demonstrates that there is no need to invoke abnormally high spin parameters to explain the scaling relations of star-forming disk-galaxies at high redshifts ($z \simeq 2$) as has been claimed by Bouché et al. (2007) and Burkert et al. (2009).

The weak evolution of the galaxy scaling relations since $z \sim 1$ in our model is due to the fact that individual galaxies grow roughly along the scaling relations, and not due to weak evolution in the properties of individual galaxies themselves. Similar conclusions for the stellar mass-velocity relation have been reached by Portinari & Sommer-Larsen (2007) using cosmological simulations, and for the size-stellar mass relation by Firmani & Avila-Reese (2009) using a semi-analytic model similar to the one used here. For example, for a galaxy with present day stellar mass of

$3 \times 10^{10} M_\odot$, since $z = 1$, its stellar mass has increased by a factor of $\simeq 2.5$, its half-light size has increased by a factor of $\simeq 2.0$, and its maximum circular velocity has increased by a factor of $\simeq 1.15$. In terms of samples of galaxies, the evolution is just a factor of $\simeq 1.5$ increase in stellar mass, at fixed V_{max} , and a factor of $\simeq 1.3$ increase in disk size at fixed stellar mass, since $z = 1$. Evolution in stellar mass by a factor of $\simeq 2.5$ for galaxies with present day stellar masses of $3 \times 10^{10} M_\odot$ is also consistent with the evolution of the star formation rate - stellar mass relation since $z = 1$ (Noeske et al. 2007b).

In our models the evolution of the stellar scaling relations is *stronger* than that of the baryonic scaling relations (maximum circular velocity, baryonic mass, baryonic half-mass size). This is due to a combination of the inside-out nature of stellar disk growth in Λ CDM cosmologies, coupled to a decrease in cold gas fractions with cosmic time.

In our models the evolution of the baryonic scaling relations is *weaker* than that of the virial scaling relations of dark matter haloes, assuming a constant galaxy mass fraction. For example, the baryonic TF and baryonic size-velocity relations evolve by just $\simeq 0.11$ dex from $z = 1$ to $z = 0$, whereas the corresponding relations between halo virial quantities evolve by $\simeq 0.33$ dex from $z = 1$ to $z = 0$. This difference can be understood as a consequence of the ratio between maximum circular velocity and virial circular velocity, V_{max}/V_{vir} , increasing towards lower redshifts. This in turn is largely a consequence of the increase in halo concentrations with time (e.g., Bullock et al. 2001a).

While we have shown that there is a consistent observational and theoretical picture for the evolution of the VMR relations out to redshift $z \sim 2$, there is much room for progress. Our theoretical model makes a number of simplifying assumptions which are unlikely to be correct in detail. We assume that the galaxy mass fraction and galaxy spin parameters do not evolve with time. While this is a reasonable assumption to start with, we note that this is not a natural outcome of our model when we include cooling and outflows. Our model also assumes that galaxy disks are smooth, and 100% supported by rotation. This assumption is valid in the local universe, and perhaps up to redshift $z \sim 1$, but may break down at higher ($z \gtrsim 2$) redshifts, especially for lower mass galaxies.

Current observational samples at $z \gtrsim 1$ are small and/or subject to measurement uncertainties and selection biases. For the RM relation, it will be possible, in the near future, to measure robust rest-frame optical sizes at $z \lesssim 2.5$ using large NIR surveys with *HST*/Wide Field Camera 3. Measuring maximum circular velocities is currently a challenge at high redshifts, as it is limited to ground based NIR spectroscopy. These observations are typically seeing limited, which complicates the measurement of maximum rotation velocities. However, coming generations of adaptive optics-assisted ground based telescopes will open up the field in concert with the Atacama Large Millimeter/submillimeter Array (ALMA) and the Square Kilometer Array (SKA). With this suite of frontier instrumentation, it will be possible to measure resolved rotation curves and gas density profiles in molecular and atomic gas out to high redshifts. Coupled to observations of stellar masses and sizes, these observations will enable the evolution of the baryonic VMR scaling relations over a large fraction of cosmic time to be

measured. These scaling relations will provide a complete set of observational constraints with which to test models of disk-galaxy formation.

ACKNOWLEDGEMENTS

We thank Nicolas Bouché for useful discussions regarding the SINS data. A.A.D. acknowledges financial support from a CITA National Fellowship, from the National Science Foundation grant AST-08-08133, and from Hubble Space Telescope grants GO-10532.02-A and GO-11206.02-A.

The DEEP2 survey was initiated under the auspices of the NSF Center for Particle Astrophysics. Major grant support was provided by National Science Foundation grants AST 95-29098, 00-711098, 05-07483, and 08-08133 to UCSC and AST 00-71048, 05-07428, and 08-07630 to UCB. The DEEP2 survey has been made possible through the dedicated efforts of the DEIMOS instrument team at UC Santa Cruz and support of the staff at Keck Observatory. The *HST* ACS mosaic in EGS was constructed by Anton Koeke-moer and Jennifer Lotz and was funded by grant HST-AR-01947 from NASA. Finally, we recognize and acknowledge the highly significant cultural role and reverence that the summit of Mauna Kea has always had within the indigenous Hawaiian community; it has been a privilege to be given the opportunity to conduct observations from this mountain.

REFERENCES

- Abazajian, K. N., et al. 2009, *ApJS*, 182, 543
- Bamford, S. P., Milvang-Jensen, B., Aragón-Salamanca, A., & Simard, L. 2005, *MNRAS*, 361, 109
- Bamford, S. P., Aragón-Salamanca, A., & Milvang-Jensen, B. 2006, *MNRAS*, 366, 308
- Barden, M., et al. 2005, *ApJ*, 635, 959
- Bell, E. F., & de Jong, R. S. 2001, *ApJ*, 550, 212
- Bell, E. F., McIntosh, D. H., Katz, N., & Weinberg, M. D. 2003, *ApJS*, 149, 289
- Blanton, M. R., & Roweis, S. 2007, *AJ*, 133, 734
- Blumenthal, G. R., Faber, S. M., Primack, J. R., & Rees, M. J. 1984, *Nature*, 311, 517
- Blumenthal, G. R., Faber, S. M., Flores, R., & Primack, J. R., 1986, *ApJ*, 301, 27
- Böhm, A., et al. 2004, *A&A*, 420, 97
- Bouché, N., et al. 2007, *ApJ*, 671, 303
- Bruzual, G., & Charlot, S. 2003, *MNRAS*, 344, 1000
- Bryan, G. L., & Norman, M. L. 1998, *ApJ*, 495, 80
- Bullock, J. S., Kolatt, T. S., Sigad, Y., Somerville, R. S., Kravtsov, A. V., Klypin, A. A., Primack, J. R., & Dekel, A. 2001a, *MNRAS*, 321, 559
- Bullock, J. S., Dekel, A., Kolatt, T. S., Kravtsov, A. V., Klypin, A. A., Porciani, C., & Primack, J. R. 2001b, *ApJ*, 555, 240
- Bundy, K., et al. 2006, *ApJ*, 651, 120
- Burkert, A., et al. 2009, arXiv:0907.4777
- Chabrier, G. 2003, *PASP*, 115, 763
- Chiu, K., Bamford, S. P., & Bunker, A. 2007, *MNRAS*, 377, 806
- Conselice, C. J., Bundy, K., Ellis, R. S., Brichmann, J., Vogt, N. P., & Phillips, A. C. 2005, *ApJ*, 628, 160
- Cresci, G., et al. 2009, *ApJ*, 697, 115
- Courteau, S. 1997, *AJ*, 114, 2402
- Courteau, S., Dutton, A. A., van den Bosch, F. C., MacArthur, L. A., Dekel, A., McIntosh, D. H., & Dale, D. A. 2007, *ApJ*, 671, 203
- Daddi, E., et al. 2010, *ApJ*, 713, 686
- Dalcanton, J. J., Spergel, D. N., & Summers, F. J. 1997, *ApJ*, 482, 659
- Davis, M., et al. 2003, *SPIE*, 4834, 161
- Davis, M., et al. 2007, *ApJL*, 660, L1
- de Jong, R. S., & Lacey, C. 2000, *ApJ*, 545, 781
- Dunkley, J., et al. 2009, *ApJS*, 180, 306
- Dutton, A. A., van den Bosch, F. C., Dekel, A., & Courteau, S. 2007, *ApJ*, 654, 27
- Dutton, A. A. 2009, *MNRAS*, 396, 121
- Dutton, A. A., & van den Bosch, F. C. 2009, *MNRAS*, 396, 141
- Dutton, A. A., van den Bosch, F. C., & Dekel, A. 2010a, *MNRAS*, 405, 1690
- Dutton, A. A., Conroy, C., van den Bosch, F. C., Prada, F., & More, S. 2010b, *MNRAS*, 407, 2
- Elmegreen, B. G., Bournaud, F., & Elmegreen, D. M. 2008, *ApJ*, 688, 67
- El-Zant, A. A., Shlosman, I., & Hoffman, Y. 2001, *ApJ*, 560, 636
- Erb, D. K., Steidel, C. C., Shapley, A. E., Pettini, M., Reddy, N. A., & Adelberger, K. L. 2006, *ApJ*, 646, 107
- Fall, S. M., & Efstathiou, G. 1980, *MNRAS*, 193, 189
- Fernández Lorenzo, M., Cepa, J., Bongiovanni, A., Pérez García, A. M., Lara-López, M. A., Pović, M., & Sánchez-Portal, M. 2010, arXiv:1005.1512, *A&A* in press
- Firmani, C., & Avila-Reese, V. 2000, *MNRAS*, 315, 457
- Firmani, C., & Avila-Reese, V. 2003, *Revista Mexicana de Astronomía y Astrofísica Conference Series*, 17, 107
- Firmani, C., & Avila-Reese, V. 2009, *MNRAS*, 396, 1675
- Flores, H., Hammer, F., Puech, M., Amram, P., & Balkowski, C. 2006, *A&A*, 455, 107
- Förster Schreiber, N. M., et al. 2009, *ApJ*, 706, 1364
- Governato, F., et al. 2010, *Nature*, 463, 203
- Hoekstra, H., Hsieh, B. C., Yee, H. K. C., Lin, H., & Gladders, M. D. 2005, *ApJ*, 635, 73
- Jardel, J. R., & Sellwood, J. A. 2009, *ApJ*, 691, 1300
- Kassin, S. A., et al. 2007, *ApJL*, 660, L35
- Kennicutt, R. C. 1998, *ApJ*, 498, 541
- Lin, L., et al. 2007, *ApJL*, 660, L51
- MacArthur, L. A., Courteau, S., & Holtzman, J. A. 2003, *ApJ*, 582, 689
- Macciò, A. V., Dutton, A. A., van den Bosch, F. C., Moore, B., Potter, D., & Stadel, J. 2007, *MNRAS*, 378, 55
- Macciò, A. V., Dutton, A. A., & van den Bosch, F. C. 2008, *MNRAS*, 391, 1940
- Maller, A. H., & Dekel, A. 2002, *MNRAS*, 335, 487
- Mao, S., Mo, H. J., & White, S. D. M. 1998, *MNRAS*, 297, L71
- Melbourne, J., Phillips, A. C., Harker, J., Novak, G., Koo, D. C., & Faber, S. M. 2007, *ApJ*, 660, 81
- Mo, H. J., Mao, S., & White, S. D. M. 1998, *MNRAS*, 295, 319
- Mo, H. J., & Mao, S. 2004, *MNRAS*, 353, 829
- Navarro, J. F., Frenk, C. S., & White, S. D. M. 1997, *ApJ*, 490, 493
- Navarro, J. F., & Steinmetz, M. 2000, *ApJ*, 538, 477
- Noeske, K. G., et al. 2007a, *ApJL*, 660, L43
- Noeske, K. G., et al. 2007b, *ApJL*, 660, L47
- Peebles, P. J. E. 1969, *ApJ*, 155, 393
- Piontek, F., & Steinmetz, M. 2009, arXiv:0909.4156
- Pizagno, J., et al. 2005, *ApJ*, 633, 844
- Portinari, L., & Sommer-Larsen, J. 2007, *MNRAS*, 375, 913
- Puech, M., et al. 2008, *A&A*, 484, 173
- Puech, M., Hammer, F., Flores, H., Delgado-Serrano, R., Rodríguez, M., & Yang, Y. 2010, *A&A*, 510, A68
- Read, J. I., & Gilmore, G. 2005, *MNRAS*, 356, 107
- Sales, L. V., Navarro, J. F., Schaye, J., Dalla Vecchia, C., Springel, V., Haas, M. R., & Helmi, A. 2009, *MNRAS*, 399, L64
- Sellwood, J. A. 2008, *ApJ*, 679, 379

- Shapley, A. E., Steidel, C. C., Pettini, M., & Adelberger, K. L. 2003, *ApJ*, 588, 65
- Sharma, S., & Steinmetz, M. 2005, *ApJ*, 628, 21
- Shen, S., Mo, H. J., White, S. D. M., Blanton, M. R., Kauffmann, G., Voges, W., Brinkmann, J., & Csabai, I. 2003, *MNRAS*, 343, 978
- Simard, L., & Pritchett, C. J. 1998, *ApJ*, 505, 96
- Simard, L., et al. 2002, *ApJS*, 142, 1
- Somerville, R. S., et al. 2008, *ApJ*, 672, 776
- Tacconi, L. J., et al. 2010, *Nature*, 463, 781
- Trujillo, I., et al. 2006, *ApJ*, 650, 18
- Tully, R. B., & Fisher, J. R. 1977, *A&A*, 54, 661
- van Dokkum, P. G., et al. 2008, *ApJL*, 677, L5
- Vogt, N. P., Forbes, D. A., Phillips, A. C., Gronwall, C., Faber, S. M., Illingworth, G. D., & Koo, D. C. 1996, *ApJL*, 465, L15
- Vogt, N. P., et al. 1997, *ApJL*, 479, L121
- Vogt, N. P., et al. 2005, *ApJS*, 159, 41
- Weinberg, M. D., & Katz, N. 2002, *ApJ*, 580, 627
- Weiner, B. J., et al. 2005, *ApJ*, 620, 595
- Weiner, B. J., et al. 2006a, *ApJ*, 653, 1027
- Weiner, B. J., et al. 2006b, *ApJ*, 653, 1049
- Weiner, B. J., et al. 2009, *ApJ*, 692, 187
- Williams, R. J., Quadri, R. F., Franx, M., van Dokkum, P., Toft, S., Kriek, M., & Labbé, I. 2010, *ApJ*, 713, 738
- Willmer, C. N. A., et al. 2006, *ApJ*, 647, 853
- White, S. D. M., & Rees, M. J. 1978, *MNRAS*, 183, 341
- York, D. G., et al. 2000, *AJ*, 120, 1579
- Ziegler, B. L., et al. 2002, *ApJL*, 564, L69